Hydrous Melting of the Metasomatized Asthenospheric Mantle Below East Asia Producing LOMU Type Alkali Basalts: New insights from Higashi-Matsuura rear-arc Basalts, Kyushu, Japan

Dey Bidisha [1,2]

Corresponding Author

Email: bidisha-dey@hiroshima-u.ac.jp

Shibata Tomoyuki [1,2]

Yoshikawa Masako [1,2]

[1] Earth and planetary systems science program, Hiroshima University, 1-3-1 Kagamiyama, Higashi-Hiroshima City, Hiroshima, 739-8526, Japan

Ph: +81-082-424-7305

[2] Hiroshima Institute of Plate Convergence Region Research, Hiroshima University, 1-3-1 Kagamiyama, Higashi-Hiroshima City, Hiroshima, 739-8526, Japan

Ph: +81-082-424-7305

ABSTRACT

Alkali basalts with distinctive time-integrated low U/Pb (low μ, LOMU) have been reported in East Asia from the arc, rear-arc, forearc and intraplate volcanoes in northeast China, Korea, Sea of Japan, and the Petit Spot near the Japan Trench. The origin of these alkali basalts in East Asia is controversial due to the complex geochemical and tectonic signatures reported from this region. We report new data on the petrology and geochemistry of the Higashi-Matsuura and Kita-Matsuura alkali basalts from southwest Japan, which confirm the presence of a LOMU-type mantle component below the Japanese islands. Petrological studies show that the Higashi-Matsuura alkali basalts (~3 Ma) were derived from a hydrous mantle source with ~1500 µg/g H_2O, at a pressure of 1.9 to 2.1 GPa. These alkali basalts show $^{206}Pb/^{204}Pb$ values of 17.72 to 18.04 which are among the lowest values from southwest Japan. Relatively older (6 - 8 Ma) alkaline basalts from the Kita-Matsuura area showing similar physicochemical characteristics do not show LOMU-type isotopic trends. Trace element and Pb-Sr-Nd isotopic data indicate that the Higashi-Matsuura mantle component is similar to the extreme LOMU components reported from the Chinese and Korean alkali basalts, as well as the recently discovered Petit Spot volcanoes on the Pacific plate. Pressure estimates and geochemical signatures suggest that these basalts were formed by the melting of an enriched asthenospheric mantle showing LOMU-like isotope ratios and melt interaction with the MORB-like subcontinental lithospheric mantle. We model the origin of the LOMU signature from the lowest reported Pb isotope ratios in East Asia, from the Xiaogulihe volcano in northeastern China. Our model suggests that at least two separate subduction events of marine sediments, at 1.8 Ga and 2.2 Ga, are required to explain the observed Pb isotopic variation in the East Asian region. Other LOMU type basalts from East Asia, including southwest Japan and Petit Spot, define a linear trend between the Xiaogulihe basalts and lithospheric mantle xenoliths. This suggests that the LOMU array in East Asia may have been formed by mixing between multiple ancient, subducted sediment components accumulated at the mantle transition zone for over 2 billion years, and its recent upwelling due to dehydration of the stagnant Pacific slab and related melting of the metasomatized asthenospheric mantle.

Keywords: Alkali basalts; East Asian mantle; LOMU; Southwest Japan

INTRODUCTION

Mantle geochemistry below the continents is difficult to determine due to the thick continental crust and its interaction with any upwelling magma. Nevertheless, attempts have been made to decipher the nature of the mantle beneath continental regions in order to understand the geochemical evolution of the Earth. The mantle below the East Asian region is of particular interest due to the complex tectonic setting and unique geochemistry of volcanic rocks found in this region. Cenozoic volcanism in northeast China and Korea comprising of ultrapotassic to alkaline basalts has been extensively studied and show ocean island basalt (OIB) like trace element patterns and enriched mantle (EM 1) like radiogenic isotope ratios (Basu *et al.*, 1991; Menzies, 1995; Chen *et al.*, 2017; Sun *et al.*, 2017; Wang *et al.*, 2017; Choi *et al.*, 2020). However, the origin of this signature is still ambiguous and thought to contain material from multiple components such as recycled sediments, oceanic crust, metasomatized asthenospheric mantle and the subcontinental lithospheric mantle (Choi *et al.*, 2006, 2020; Chen *et al.*, 2007; Kuritani *et al.*, 2009, 2011; Sun *et al.*, 2017; Wang *et al.*, 2017; Shi *et al.*, 2023). Some Cenozoic alkali basalts from southwest Japan showing similar trace element patterns have also been reported to contain low radiogenic Pb compared to arc basalts (Tatsumoto, 1969) and later linked to enriched mantle 1 or EM 1 (Zindler, 1986) type mantle component (Tatsumoto and Nakamura, 1991). Although high $^{3}He/^{4}He$ in Takashima xenoliths from southwest Japan suggest a contribution from primitive lower mantle (Sumino *et al.*, 2000), plume from the lower mantle have not been observed in seismic studies in the area. Rather, the presence of the stagnant Pacific plate at the mantle transition zone (Fukao *et al.*, 1992; Richard and Iwamori, 2010; Zhao *et al.*, 2012a; Huang *et al.*, 2013), and a lack of a high $^{3}He/^{4}He$ in mantle xenoliths from northeast China (Chen *et al.*, 2007), suggests against any upwelling from the lower mantle below East Asia. Contribution from enriched mantle components (both EM 1 and EM 2) to the basalts of southwest Japan have been proposed in the past based on their radiogenic isotope geochemistry (Tatsumoto and Nakamura, 1991; Hoang and Uto, 2003, 2006). The source of the EM 1 signature has been suggested to originate from ancient subducted sediments based on radiogenic and stable isotope ratios (Eisele *et al.*, 2002; Kuritani *et al.*, 2011; Wang *et al.*, 2017; Shi *et al.*, 2023). Recent research using non-traditional stable isotopes suggest deep subduction of ancient carbonate sediments contributing to the time integrated low U/Pb bearing EM 1 signature from northeast China, correlated to low δ^{26}Mg, δ^{57}Fe, $\delta^{44/40}$Ca and high δ^{66}Zn (Li *et al.*, 2017; Sun *et al.*, 2017; Wang *et al.*, 2017; Liu and Li, 2019; Wei *et al.*, 2021; Shi *et al.*, 2023). However (Choi and Liu, 2022) argue for a Paleoproterozoic siliciclastic source for the EM 1 component in Changbaishan basalts, based on Pb-Mg-Zn isotope systematics with contribution from carbonated eclogite from the stagnant Pacific plate. Interestingly, similar isotopic signature with low radiogenic Pb have been reported from the recently discovered Petit Spot volcanoes (Fig. 1a) near the Japan Trench (Machida *et al.*, 2009; Liu *et al.*, 2020; Hirano and Machida, 2022). The geochemical signatures of these basalts differ from the northeast China EM 1 basalts to some extent and their genesis have been explained by mixing with ancient carbonated eclogites in the asthenospheric mantle (Liu *et al.*, 2020). Hance, the possible heterogeneous distribution of multiple EM 1 sources in the mantle below East Asia present an enigma for the evolution of the EM 1 signature in this area. Until now, Investigation on the source and nature of the continental EM 1 mantle below East Asia has been focused on volcanoes from northeast China and Korea. In this study we investigate the mantle heterogeneity below southwest Japan using petrological, trace elemental, and Pb-Sr-Nd isotope ratios from Kita-Matsuura and Higashi-Matsuura alkali basalts. Furthermore, we re-evaluate the genetic model for EM 1 signature from East Asia by modelling the radiogenic evolution and mixing in Pb isotope space.

GEOTECTONIC BACKGROUND

The Japanese islands are situated at the junction of three major tectonic plates. The Pacific Plate is subducting beneath the Eurasian Plate at the Japan Trench and the Philippine Sea (PHS) Plate at the Izu-Bonine-Mariana Trench. The Philippine Sea Plate is in turn subducting beneath southwest Japan at the Nankai Trough and Ryukyu Trench (Fig. 1a). Arc and rear-arc volcanoes resulting from the subduction settings are seen all along Japan. Intraplate volcanoes unrelated to these subduction settings, are also found further west of the plate boundary in Jeju island and northeast China at Xiaogulihe, Wudalianchi, Erkeshan etc. (Kamata and Kodama, 1999; Choi *et al.*, 2006, 2020; Sakuyama *et al.*, 2014b; Shibata *et al.*, 2014; Sun *et al.*, 2014; Wang *et al.*, 2017).

The subducted Pacific slab is stagnant at the 660 km discontinuity at the bottom of the upper mantle (Zhao *et al.*, 2012a), above which the Philippine sea plate is presently subducting below southwest Japan and has reached up to the Goto islands (Huang *et al.*, 2013). A buoyant hydrous plume generated from the stagnant Pacific slab is inferred to be present below the East Asian region (Richard and Iwamori, 2010; Huang *et al.*, 2013; Sakuyama *et al.*, 2013; Kuritani *et al.*, 2017). The southwest Japan arc extends NNE-SSW from southern Honshu (Daisen, Abu) to central Kyushu (Aso, Kuju) (Fig. 1b), and Cenozoic volcanism from about 15 Ma to recent can be seen in the arc and rear-arc region. Subduction related volcanism prior to 15 Ma is the effect of the Pacific plate subducting beneath Eurasian plate and later volcanism (< 6 Ma) is related to the subduction of the Philippine Sea plate below Kyushu (Kamata and Kodama, 1999; Mahony *et al.*, 2011). The basalts analysed were sampled from the Kita-Matsuura and Higashi-Matsuura volcanic fields (Fig. 1c) of northwestern Kyushu, where basaltic volcanism is present from 6.11 to 8.63 Ma for Kita-Matsuura (Sakuyama *et al.*, 2009) and 2.92 to 3.01 Ma for Higashi-Matsuura (Nakamura *et al.*, 1986).

The alkali olivine basalts in this study were collected from the Kita-Matsuura and Higashi-Matsuura region of southwest Japan. Kita-Matsuura samples were collected from Ikitsuki island and Tabiracho area, and Higashi-Matsuura samples were collected near Genkaicho and Karatsushi. Sample locations are shown in Fig. 1c, and GPS coordinates are represented in Table 1.

MATERIALS AND METHODS

Alkali basalts from Kita-Matsuura and Higashi-Matsuura were sampled from the field for petrological and geochemical studies. Thin sections were prepared, polished, and studied under polarising microscope and scanning electron microscope (SEM) at the Hiroshima University. Modal abundances were estimated by image analysis of ~1.5 cm^2 area of SEM images per thin section, using 'ImageJ' software. Chemical compositions of minerals were analysed using Electron Probe Microanalyzer (EPMA) of the model JEOL JXA-isp100 situated at the Hiroshima University. Samples were measured at an accelerating voltage of 15 kV and beam current of 10 nA. A probe diameter of 3 μm was used for olivine and clinopyroxene, and 5 μm was used for plagioclase. Mineral and oxide standards were used for calibration and data was obtained after ZAF correction.

All rock samples were crushed to coarse chips (≈0.5 cm^3) using a jaw crusher prior to whole-rock geochemical and Sr-Nd-Pb isotopic analyses. Fresh pieces without saw marks were handpicked for grinding and were rinsed with ethanol and Milli Q water in an ultrasonic bath to avoid surface contamination. The cleaned and dried rock chips were then ground to a grain-size of less than 200 mesh using a vibrating tungsten carbide puck mill. Glass beads were prepared, and major element and selected trace element compositions were determined using XRF (Rigaku ZSX-Primus II) installed at the Hiroshima University, following

Kanazawa et al., (2001). Powdered samples were digested with HF, $HClO_4$ and HCl in a class 1000 clean room on a class 10 clean bench for trace element and isotopic analyses. Trace element compositions were determined by diluting the digested rock powders with 5% m/v HNO_3 and analysis in a inductively coupled plasma mass spectroscopy (ICP-MS) of the model Thermo Scientific X Series-2 installed at the Hiroshima University (Chang *et al.*, 2002). Elemental separation for isotope ratio analysis were done from part of the digested sample. Pb, Sr and Nd were separated using a sequential column chemistry method following Dey et al. (2023).

Pb-Sr-Nd isotope ratios were determined using a thermal ionisation mass spectrometer (TIMS) from Thermo Scientific (MAT-262), equipped with nine faraday cups, installed at the Hiroshima University (Shibata *et al.*, 2014; Dey *et al.*, 2023). Instrumental mass fractionation was corrected by internal normalization for Sr and Nd with $^{86}Sr/^{88}Sr = 0.1194$ (Birck, 1986) and $^{146}Nd/^{144}Nd = 0.7219$ (Depaolo, 1988). Pb isotopic fractionation was corrected using double spike method with two separate measurements of unspiked and double spiked fractions (Compston and Oversby, 1969). Accuracy of measurement was confirmed by repeated measurements of isotope references for Sr, Nd and Pb. NIST SRM 987 provided an $^{87}Sr/^{86}Sr$ ratio of 0.710264 ± 0.000014 (2σ, n = 10) while La Jolla Nd standard provided a $^{143}Nd/^{144}Nd$ ratio of 0.511853 ± 0.000011 (2σ, n = 10). Double spike corrected values for NIST SRM 981 were measured as $^{206}Pb/^{204}Pb = 16.9397 \pm 0.0013$; $^{207}Pb/^{204}Pb = 15.4972 \pm 0.0013$ and $^{208}Pb/^{204}Pb = 36.7187 \pm 0.0024$ (2σ) for an average of five measurements.

RESULTS

Petrography and mineral chemistry

All samples consist of fine-grained (< 500 μm), holocrystalline basalts; with olivine, clinopyroxene, and plagioclase microphenocrysts in a plagioclase, orthopyroxene, and opaque bearing groundmass (Fig 2). Little to no alteration was observed in hand specimens and thin sections.

Samples from Kita-Matsuura (TBR-2) contain large (~1 to 0.4 mm) olivine and clinopyroxene phenocrysts, in a medium grained (~500 to 200 μm), plagioclase-bearing groundmass. with a total phenocryst abundance of ~31 vol%. Compositional zoning is visible in both olivine and clinopyroxene phenocrysts in polarising microscope and SEM (Fig. 2a, b). The forsterite content of olivine ranges from Fo_{85}- Fo_{87} in the core to ~Fo_{62} at the rim. Anorthite content for plagioclase microphenocrysts ranges from An_{59} to An_{65}. Olivine and clinopyroxene grains are clustered together and show resorbed grain boundaries in contact with plagioclase (Fig. 2a).

Higashi-Matsuura basalts contain small to medium (50 to 500 μm) olivine grains (5 to 15 vol%) in a fine-grained plagioclase and orthopyroxene bearing groundmass along with small grains of Fe-Ti oxides (~5 vol%). Phenocryst phases are dominated by olivine with minor presence (<5 vol%) of clinopyroxene. Some olivine phenocryst grains are fractured and partially altered along fractures (Fig. 2b). Unlike the Kita-Matsuura samples, the olivine grains in Higashi-Matsuura samples do not show pronounced compositional zoning, with forsterite content ranging from Fo_{70} to Fo_{80}. Plagioclase microphenocrysts show anorthite contents ranging from An_{60} to An_{69}. A large plagioclase xenocryst (~1.5 mm) with resorbed grain boundary (Fig. 2c) shows anorthite content of An_{32} to An_{45}. Proportion of glass is non-existent or negligible in all samples, in agreement with previous observations by Nakamura et al. (1986). Presence of ultramafic xenoliths and xenocrysts has been reported in Higashi-Matsuura basalts (Nakamura *et al.*, 1986) but was not observed in the samples in this study.

Whole rock major and trace element compositions

Whole rock geochemical data of the measured samples are presented in Table 1. Measured data plot in tholeiitic to alkaline range in the basalt to trachy-basalt field in a total alkali vs silica diagram (Fig. 3a; Le Bas et al., 1986). CIPW norm were calculated on anhydrous basis after redistribution of FeO(t) according to $Fe^{+2}/Fe^{+3} = 0.8$ (Table 2). Kita-Matsuura samples show 11 to 14% normative olivine (Ol) and 2.4 to 10.8% normative hypersthene (Hyp). Normative Ol and Hyp content are 12.6 to 16.2% and 0 to 5.6% for Higashi-Matsuura samples. One sample shows normative nepheline of 0.7%.

Samples were plotted in the geotectonic classification scheme for tholeiitic and alkaline rocks (Pearce and Cann, 1973) using immobile trace element data (Fig. 3b). Samples from Kita-Matsuura plot near the boundary of within-plate basalts and calc-alkaline basalts while the samples from Higashi-Matsuura plot in the within-plate basalt field. One sample from Higashi-Matsuura (HDO-2) was excluded from the classification due to anomalously high Y concentration. Primitive mantle normalized trace element diagram (Fig. 3c) and Chondrite normalized rare earth elements (REE) diagram (Fig. 3d) show similar patterns to ocean island basalts (OIB). Depletion of high field strength elements (HFSE), which is a common trait for arc and rear-arc basalts are absent for all the samples for Higashi-Matsuura while the samples from Kita-Matsuura show weak depletion of Nb. One sample (HDO-2) deviate from the common trend with enriched heavy rare earth and Y. Rhabdophane, an Y bearing phase was reported from Higashi-Matsuura basalts from the Genkaicho region (Takai and Uehara, 2012) which may explain the enriched Y and HREE in this sample. HFSE concentrations are significantly higher for all samples, with Nb ranging from 11 to 44 μg/g, compared to MORB or typical arc basalts (<5 μg/g). Ba, K, Pb and Sr show enriched pattern in trace element diagram. One sample from Kita-Matsuura (TBR-2) show high Ni (206 μg/g) and Cr concentration (479 μg/g) compared to other samples (<100 and <300 μg/g respectively) which may suggest relatively low mineral fractionation from primary magma. Chondrite normalized rare earth element pattern shows enrichment in light rare earths compared to heavy rare earths.

Pb-Sr-Nd isotope compositions

$^{87}Sr/^{86}Sr$, $^{143}Nd/^{144}Nd$, $^{206}Pb/^{204}Pb$, $^{207}Pb/^{204}Pb$ and $^{208}Pb/^{204}Pb$ ratios are presented in Table -2, and isotope diagrams are plotted in Fig. 4. $^{87}Sr/^{86}Sr$ and $^{143}Nd/^{144}Nd$ isotope ratios range between 0.7039 and 0.7044 and 0.51267 and 0.51279 respectively which are enriched compared to the depleted mantle and MORB (Fig. 4a). Higashi-Matsuura samples show relatively more enriched Sr-Nd isotope ratios compared to Kita-Matsuura, while the reverse trend is seen for Pb isotope ratios. Measured data from Kita-Matsuura fall within previously reported values (Fig. 4). Higashi- Mastuura samples show low radiogenic $^{206}Pb/^{204}Pb$ compared to previously reported data from Kyushu (Hoang and Uto, 2006), with $^{206}Pb/^{204}Pb$ between 17.72 to 18.04. $^{207}Pb/^{204}Pb$ and $^{208}Pb/^{204}Pb$ do not show such distinct difference from previously reported data, and range between 15.44 to 15.57 and 38.06 to 38.40 respectively. One sample from Higashi-Matsuura (HDO-2) show enrichment in HREEs compared to the other Higashi-Matsuura samples indicate possible contamination during magma ascent or involvement of a distinct component in the source material. However, the Pb-Sr-Nd isotope ratios do not show significant variation from the other samples of Higashi-Matsuura indicating that the Pb-Sr-Nd budget is not affected due to the contamination.

DISCUSSION

Physicochemical characteristics of the basaltic melt and inferred primary magma

Primary magma of basaltic nature is generally generated by decompression or fluid induced melting of the mantle (Tatsumi *et al.*, 1983; Wilson, 1989). Subsequent fractionation of minerals like olivine, clinopyroxene and plagioclase from the primary mantle melt, during ascent and cooling (Pearce, 1978; Tatsumi *et al.*, 1983), and assimilation of wall rock during ascent (DePaolo, 1981), may also change the composition of the magma before eruption and solidification. Such signatures are often decipherable from the petrographic features and chemical composition of the basalts. In the following section, we attempt to decipher the physicochemical nature of the basaltic magmas and their parent primary magmas.

Higashi-Matsuura

Higashi-Matsuura alkali basalts exhibit low SiO_2 (47 to 48.2 wt%), with relatively high K_2O (1.5 to 1.9 wt%) and Na_2O (2.9 to 4 wt%) content (Table 1). MgO content varies between 4.4 to 7.4 wt% with two samples (GNK-2 and Kaga-2) showing the highest abundances (~7.4 wt%). These two samples also show the highest Ni (~100 μg/g) and Cr (217 to 280 μg/g) content suggesting that these may be the most primitive samples analysed for Higashi-Matsuura basalts. Tatsumi *et al.* (1983) suggested that primary magma in equilibrium with the mantle shows an FeO(t)/MgO ratio less than unity. However, both of the samples show FeO(t)/MgO >1 which suggests that they are not primary basalts, but some amounts of mineral fractionation have taken place. Arc and rear-arc basalts often produce negative Eu anomaly in the chondrite normalised REE diagram due to fractionation of plagioclase in which Eu is strongly partitioned into plagioclase unlike other REEs. Assimilation of wall rock would produce the reverse effect and show a positive Eu anomaly in the chondrite normalised REE pattern. The absence of significant Eu anomaly in the chondrite normalized REE diagram (Fig. 3d) suggests an insignificant plagioclase fractionation or crustal assimilation for these rocks. Mineral chemistry analysed for one of the samples (GNK-2) show a highest Fo# content of 80.5 as opposed to mantle olivine with Fo_{89}, suggesting that olivine fractionation may have taken place.

Crystallization conditions and water content of the basaltic magma was calculated for GNK-1 and GNK-2 using mineral chemistry data and clinopyroxene thermobarometry (Wang *et al.*, 2021) and hygrometry (Perinelli *et al.*, 2016). The pressure, temperature and H_2O content was simultaneously solved using the SOLVER function of Excel. Results suggest that core of one relatively larger, euhedral Cpx was in equilibrium with a deeper (~0.6 GPa), hotter (1180 °C) and dryer (1.3 wt% H_2O) melt, compared to smaller Cpx grains and rim of large grain (~0.2 GPa, 1090 °C, 2.0 wt% H_2O). Cpx saturation temperature (eq. 34, Putirka, 2008) of 1181 °C, calculated for the magma composition equivalent to the whole rock at 0.6 GPa and 1.3 wt% H_2O also agrees to the Cpx core temperature, suggesting that the core is in equilibrium with the whole rock composition. H_2O content in equilibrium with Cpx ranged from 1.9 to 2.3 wt% for GNK-2, with an average of 2.0 wt% for Cpx excluding one phenocryst core (1.3 wt%). Cpx in groundmass of GNK-1 yielded equilibrium temperatures of ~1090°C at low pressure (<0.05 GPa) and 0.7 to 1.1 wt% H_2O which indicates degassing at near surface conditions. Whole rock $Fe^{2+}/(Fe^{2+} + Fe^{3+}) = 0.8$ was selected following an estimates for ~2.0 wt% H_2O by Kelley et al. (2006).

The most primitive samples, GNK-2 and Kaga-1 were selected for calculation of primary melt based on highest MgO content (~7.4) and high Ni and Cr abundances. It is assumed olivine has fractionated without significant clinopyroxene fractionation from the primary melt as Cpx phenocryst core is in equilibrium with the whole rock composition. The highest measured Fo# of olivine core ($Fo_{80.5}$) is fairly close to olivine in equilibrium with the whole rock composition (Fo_{85}) and mantle olivine (Fo_{89}), considering an olivine/ melt partition coefficient $(Fe^{2+}/Mg)^{olivine/melt} = 0.3$ (Roeder and Emslie, 1970). Insignificant plagioclase fractionation can be inferred based on insignificant Eu anomaly in chondrite normalized REE diagram (Fig. 3d). The primary magma composition for these basalts were calculated using the olivine maximum fractionation model by addition of 0.5 wt% equilibrium olivine (Roeder and Emslie, 1970) in each step following Tatsumi et al. (1983). Primary magma composition was determined for Kita-Matsuura samples after olivine addition up to equilibrium olivine with Fo_{90}, as the source mantle for Kyushu rear-arc basalts is likely to be refractory as demonstrated by mantle xenoliths hosted by Takashima and Fukuejima basalts (Sakuyama *et al.*, 2009). The calculated primary melts are obtained after addition of 13.5 and 16 wt% equilibrium olivine for GNK-2 and Kaga-1 respectively. SiO_2 content of primary magma is 48.6 and 47.9 respectively. H_2O content of primary magma was calculated to be ~1.8 wt% by assuming a constant H_2O/K_2O during crystal fractionation (Kuritani *et al.*, 2017). Composition of primary magmas and corresponding normative compositions are given in Table 3.

Kita-Matsuura

The three measured samples from Kita-Matsuura exhibit low SiO_2 (48.6 to 49 wt%) and relatively high MgO content (6.7 to 9.5 wt%). The FeO(t)/MgO ratios for these samples (1.02 to 1.27) suggests that these are not primary melt, rather may have formed by olivine fractionation from primary melt.

Crystallization pressure, temperature and water content for basaltic melt was calculated for TBR-2, using Cpx thermobarometry and hygrometry similar to Higashi-

Matsuura. Results suggests an H_2O content of ~2.3 wt% ± 0.6 wt% (2σ, n = 12) for calculated pressures ranging from 0.4 to 0.05 GPa and temperatures ranging from 1070 to 1130 °C. The clinopyroxene saturation temperature of ~1165 °C for the whole rock composition (eqn. 34, Putirka, 2008) also agree to the crystallization temperatures. Highest measured Fo# for olivine core is 87 which is in equilibrium with the whole rock composition considering an olivine/melt partition coefficient $(Fe^{2+}/Mg)^{olivine/melt} = 0.3$ (Roeder and Emslie, 1970). Whole rock $Fe^{2+}/(Fe^{2+} + Fe^{3+}) = 0.8$ was selected following estimates for ~2.3 wt% H_2O by Kelley et al. (2006). As the highest measured Fo# for olivine core is 87 which is fairly close to that of mantle olivine (Fo_{89}), we assumed that only olivine has fractionated from the primary magma. The primary magma composition for these basalts were calculated following a similar method as for Higashi-Matsuura basalts. Primary magma composition was calculated to contain 49.5 to 49.7 wt% SiO_2 after an addition of 6 to 11 wt% equilibrium olivine. Water content of primary magma was calculated to be ~2.2 wt% following similar methods to Higashi-Matsuura basalts. The relative uniformity in primary magma composition (e.g., SiO_2, MgO content; Table 4) of the three samples from Kita-Matsuura suggest that they are generated under similar conditions and undergone varied degrees of fractionation during upwelling.

Physicochemical conditions of the source mantle

Melting depths for primary magma generation were estimated using results compiled by Sakuyama et al. (2009). Isopleths for mantle melting in the normative Ne′-Ol′-Qtz′ diagram of Irvine and Baragar, (1971) were used to determine depth of melting from calculated primary magma composition, following similar methods to Sakuyama et al. (2014b). Ne′, Ol′ and Qtz′ were calculated from the CIPW norm (Table 4) using calculated primary magma compositions using the formula Ne′ = nepheline + 0.6 × albite; Qtz′ = quartz + 0.4 × albite + 0.25 ×

orthopyroxene, and Ol′ = olivine + 0.75 × orthopyroxene (Irvine and Baragar, 1971). The results plotted in Fig. 5 show that the primary magmas of Kita-Matsuura basalts are plotted near the isopleths between 1.3 and 1.5 GPa, while the Higashi-Matsuura primary magmas are plots at the 1.6 and 1.8 GPa isopleths. Corrections in melting pressure for water content were made according to the linear interpolation of $P^{wet} = P^{dry} + H_2O^{primary} \times 0.167$ (Sakuyama *et al.*, 2014b), resulting in a melting pressure of 1.7 to 1.9 GPa for Kita-Matsuura and 1.9 to 2.1 GPa for Higashi-Matsuura. The results suggest a deeper melting depth for Higashi-Matsuura basalts compared to Kita-Matsuura. Mantle melting temperatures were estimated using the pMELTS mode (v5.6.1) in the online ENKI portal (Ghiorso *et al.*, 2002) at the calculated pressures and H_2O contents. The melting temperatures for Kita-Matsuura primary magmas were calculated to be between 1333 to 1358 °C while Higashi-Matsuura magmas yielded 1376 and 1408 °C for GNK-2 and Kaga-1 respectively. The calculated pressure and temperatures are plotted in Fig. 6, which show a linear trend connecting primary magma conditions and Cpx crystallization pressure temperatures after olivine fractionation.

The H_2O/Ce value of the source mantle is estimated to be ~380 for Higashi-Matsuura and ~415 for Kita-Matsuura, assuming that this value does not change significantly during mantle melting and fractional crystallisation (Michael, 1995). This value is higher than MORB (100- 250) (Michael, 1995) and depleted mantle (~150) (Salters and Stracke, 2004) but is lower than subduction zones (>750) (Cooper *et al.*, 2012) and Fukuejima basalts (~650) (Kuritani *et al.*, 2017). Degree of melting of the source mantle was calculated to be 8.5% for Higashi-Matsuura and 11.5% for Kita-Matsuura, assuming fractional melting (Herzberg and O'hara, 2002) of a source mantle composition of Kr4003 (Walter, 1998) and 0.04 as the partition coefficient of Ti (Kelley *et al.*, 2006). H_2O content in the source mantle was determined to be ~1530 to for Higashi-Matsuura and ~2520 µg/g for Kita-Matsuura source mantle, based on the bulk distribution coefficient of 0.012 of H_2O in the mantle (Kelley *et al.*, 2006). This water content is much higher than the MORB source mantle (50-200 μg/g) or OIB source mantle (300- 1000 μg/g) (Hirschmann, 2006), and corroborates the hypothesis of a hydrous asthenospheric mantle below Kyushu (Sakuyama *et al.*, 2014b; Kuritani *et al.*, 2017) and East Asia (Chen *et al.*, 2015, 2017; Liu *et al.*, 2017).

The estimated melting pressures for the Kita-Matsuura and Higashi-Matsuura basalts indicate that these were generated from the bottom of the lithosphere to the top of the asthenospheric mantle, considering that the lithosphere-asthenosphere boundary is at a depth of 60-65 km (~1.8 GPa) beneath northern Kyushu (Li, 2010). A 3-D P-wave velocity model by Huang et al., (2013) shows a low velocity zone below western Kyushu at a depth of 60 to 200 km. Previous research by Sakuyama et al. (2014b) from Kita-Matsuura reported water contents ranging from 0.2 to 2.3 wt%, melting pressures of 1.5 to 2.8 GPa and temperature of 1350 to 1500 °C. Relatively younger (<1 Ma) alkali basalts from Fukuejima were also reported to have formed at a melting pressure of 1.8 to 2.6 GPa and 1285 to 1345 °C (Kuritani *et al.*, 2017) suggesting continuous mantle melting near the lithosphere- asthenosphere boundary for over 8 million years. Given the hydrous nature of the mantle source coupled with melting in the upper part of the asthenospheric mantle, it is likely that a hydrous upwelling is responsible for the magmatism in this area. A similar explanation from previous studies from western Kyushu, which reported progressive, fluid fluxed melting of the asthenospheric mantle due to upwelling from the hydrous transition zone since the late Miocene (Sakuyama *et al.*, 2009, 2014b; Kuritani *et al.*, 2017), is consistent with this hypothesis. Kuritani et al., (2017) suggest that multiple phases of hydrous upwelling and mantle melting have occurred in southwest Japan since the stagnation of the Pacific plate at the mantle transition zone. Considering the spatial distance and temporal separation between Kita-Matsuura (~6 to 8 Ma), Higashi-Matsuura (~3 Ma) and Fukuejima (0.5 Ma), it is likely that all of these volcanisms are separate events of hydrous upwelling and/or melting of the metasomatized asthenospheric mantle.

Contribution from enriched component

The radiogenic isotopic ratios of Higashi-Matsuura basalts are enriched compared to the Indian and Pacific type MORB and depleted MORB mantle (DMM). However, the measured ratios plot away from the general trend shown by other Kyushu rear-arc basalts and plot towards the East Asian EM 1 or LOMU type basalts as shown in Fig. 4. Isotopic ratios from subducting sediments are also shown in Fig. 4b and d, which plot away from the Higashi-Matsuura data indicating lack of sediment input in these basalts. Enrichment in TiO_2 and K_2O for Higashi-Matsuura are inversely correlated to $^{206}Pb/^{204}Pb$ (Fig. 7) and show similar trend to alkali basalts from East Asia and Petit Spot.

East Asian alkali basalts from northeast China and Korea have been conclusively inferred to have been generated due to asthenospheric melting triggered by hydrous upwelling from the stagnant Pacific slab and melt interaction with the subcontinental lithospheric mantle (SCLM) (Kuritani *et al.*, 2011, 2013; Sakuyama *et al.*, 2014a; Wang *et al.*, 2017; Choi *et al.*, 2020). A similar mechanism of magma generation is also suggested for Petit Spot on the Pacific slab (Liu *et al.*, 2020). Ultrapotassic rocks from the Xiaogulihe volcano in northeast China are on the other hand inferred to have originated from the refractory lithospheric mantle which is metasomatized by carbonatitic melts (Weng *et al.*, 2022). The isotopic similarity between the Higashi-Matsuura alkali basalts and the LOMU type alkali basalts from East Asia suggests that a similar source may be responsible for the isotopic enrichment in the asthenospheric mantle below East Asia.

A deeper melting (~2.5 GPa) of the enriched asthenospheric mantle facilitated by hydrous upwelling over the stagnant Pacific slab has been suggested by many researchers in this area (Kuritani *et al.*, 2011, 2013, 2017, 2019; Sakuyama *et al.*, 2014b, 2014a; Sun *et al.*, 2014; Chen *et al.*, 2017; Wang *et al.*, 2017; Choi *et al.*, 2020). Apart from showing a hydrous mantle source for Kita-Matsuura, A moderate depletion of Nb for Kita-Matsuura samples in the primitive mantle normalized trace elements pattern (Fig. 3c) suggest the involvement of subduction related magmatism. Isotopic data support this hypothesis as seen in Fig. 4. A high $^{87}Sr/^{86}Sr$ and $^{206}Pb/^{204}Pb$ isotopic signature reported in previous studies (Uto *et al.*, 2004; Sakuyama *et al.*, 2014b) corresponding to siliciclastic sediment is seen for Kita-Matsuura (Fig. 4c, d). However, the lack of significant Nb depletion in Higashi-Matsuura samples as seen in Fig. 3c, suggest against involvement of a subduction related component.

Enrichment in fluid mobile elements such as Sr, Pb Ba, Rb etc. are visible as peaks in the primitive mantle normalized trace element patterns in Fig. 3c. This may occur due to fluid induced melting of the mantle wedge during the subduction of the Philippine sea plate. However, in such a case, a sediment derived Pb and Sr isotope signature is expected in the basalts. But such a signature is not evident from the low radiogenic Pb, and moderate radiogenic Sr isotopic data analysed in this study (Table 3, Fig. 4).

Higashi-Matsuura basalts show inverse correlation in $^{206}Pb/^{204}Pb$ isotope and fluid mobile elements (e.g., K, Ba, Pb, Sr) plot in Fig. 7a, c and d, while a similar trend is seen for northeast China intraplate basalts and Petit Spot basalts. This suggests that the source of these elements is correlated to a LOMU like component for Higashi-Matsuura. Previously reported data for $\delta^{26}Mg$ from northeast China alkali basalts are correlated to K_2O content as well as $^{206}Pb/^{204}Pb$ suggesting that the source of correlated low radiogenic Pb and high radiogenic Sr is likely to be carbonate sediments subducted into the mantle ~2 billion years ago (Kuritani *et al.*, 2011, 2017; Sun *et al.*, 2014, 2017; Wang *et al.*, 2017). Models by previous researchers

(Kuritani *et al.*, 2011, 2017; Sakuyama *et al.*, 2014a, 2014b; Sun *et al.*, 2014, 2017; Wang *et al.*, 2017) suggest that a region metasomatized by ancient sediments is present above the mantle transition zone in the asthenospheric mantle. Melting induced by dehydration from the stagnant Pacific slab below East Asia is responsible for transporting material from the deep metasomatized mantle and producing LOMU like isotopic signature at the northeast China region. The current study confirms the presence of ancient sediment (LOMU) like component below southwest Japan, suggesting that the metasomatized zone may be distributed throughout the mantle transition zone below east Asia, similar to northeast China and Korean volcanoes like Chugaryong, Changbaishen, Wudalianchi, Xiaogulihe etc. The lack of such signatures in other regions such as Kita-Matsuura may suggest that the asthenospheric mantle is isotopically heterogeneous below southwest Japan.

Mafic and ultramafic xenoliths from southwest Japan are plotted in Fig. 4a, and show $^{87}Sr/^{86}Sr$ and $^{143}Nd/^{144}Nd$ isotope ratios similar to southwest Japan back arc basalts (Kagami *et al.*, 1993; Ikeda *et al.*, 2001; Senda *et al.*, 2007; Yoshikawa *et al.*, 2010). but it is difficult to determine whether these are the source of isotopic variation in the observed data due to lack of reported Pb isotopic data from the xenoliths. (Hoang and Uto, 2003, 2006) suggested that the subcontinental lithospheric mantle (SCLM) below Kyushu is likely to be similar to EM 2 based on Sr and Nd isotopic data. Pb isotopic data of mantle xenoliths from Korea were reported by (Choi *et al.*, 2005) which show similar ratios to Fukuejima basalts (Kuritani *et al.*, 2017). Mixing between the LOMU source and SCLM was suggested for alkali basalts from northeast China showing LOMU like character (Wang *et al.*, 2017; Choi *et al.*, 2020). A similar trend is also visible for alkali basalts from Kyushu suggesting that the LOMU trend in southwest Japan may have originated by the mixing of deep, asthenospheric melt and the subcontinental lithospheric mantle.

Origin of LOMU component in the East Asian mantle

The source and origin of the EM 1 or LOMU signature has been discussed by various researchers and speculated to be originated either in the subcontinental lithospheric mantle (SCLM) (Basu *et al.*, 1991; Zhang *et al.*, 1995; Zou *et al.*, 2003) or in the asthenospheric mantle (Kuritani *et al.*, 2011, 2017; Sakuyama *et al.*, 2014a; Wang *et al.*, 2017). Recent research involving stable Mg, Ca, and Fe isotopes have effectively established the origin of northeast China LOMU signature to be from an ancient, subducted carbonate sediment rich region in the asthenospheric mantle (Sun *et al.*, 2017; Wang *et al.*, 2017; Wei *et al.*, 2021; Shi *et al.*, 2023). A geochemical evolution model for developing this signature was reported by Wang et al. (2017) which suggests the subduction of carbonate sediments at 2.2 Ga and subsequent evolution in the mantle with low U/Pb ratio to develop the extreme LOMU ratios for this area. This model also explains the linear trend for East Asian LOMU basalts as a mixing between a LOMU component and EM 1 type mantle signature shown by OIBs. Although this model seems to be accurate, it is unable to explain the linear trend for Xiaogulihe samples which are the extreme endmembers for the East Asian LOMU signature. Furthermore, $^{208}Pb/^{204}Pb$ isotopic signature for Pitcairn basalts, type area of EM 1, are much higher than the East Asian LOMU samples and do not fall in the same mixing trend. Isotopic diagrams suggest (Fig. 8) that ultrapotassic rocks and alkali basalts from Xiaogulihe, Nuominhe, Erkeshan, Keluo, Wudalianchi, Changbaishan (Sun *et al.*, 2014, 2017; Wang *et al.*, 2017; Kuritani *et al.*, 2019) define a quadrilateral distribution in $^{206}Pb/^{204}Pb$- $^{207}Pb/^{204}Pb$-$^{208}Pb/^{204}Pb$ space with the Xiaogulihe ultrapotassic rocks defining one edge and the Kyushu alkali basalts at the other end. Analysed samples from Higashi-Matsuura (this study), alkali basalts from petit spot near the Japan Trench (Liu *et al.*, 2020), and Goto islands (Hoang *et al.*, 2013; Kuritani *et al.*, 2017) also fall in the same plane. However, basalts from EM 1 type area, Pitcairn, do not. This suggests at least two different components may be mixing to provide the low radiogenic Pb signature for this region, which is distinctly different from the Pitcairn basalts. Therefore, we define the EM 1 type Cenozoic alkali basalts ultrapotassic rocks from northeast China, Korea, and southwest Japan as 'East Asian low μ' (EALM) basalts and attempt to re-evaluate the Pb isotopic evolution model based on a revised BSE model to explain these signatures.

Pb isotopic model

Pb is an element consisting of three radiogenic and one non radiogenic isotope in nature. ^{206}Pb and ^{207}Pb are the radiogenic daughters of ^{238}U and ^{235}U respectively, while ^{208}Pb is the radiogenic daughter of ^{232}Th. ^{204}Pb which is the least abundant among the four, is considered non-radiogenic in geologic timescale and used as the denominator to express Pb isotope ratios. Radiogenic isotope ratios in a closed system are dependent only on the parent-daughter ratio, initial ratio of the daughter isotopes, and time. Although no natural system is truly closed, we can consider a component as a closed system for the purpose of geochemical modelling unless significant mixing or fractionation between parent and daughter element has occurred during the considered time. The fact that two different variables i.e., $^{206}Pb/^{204}Pb$ and $^{207}Pb/^{204}Pb$ are dependent on three parameters i.e., U/Pb ratio denoted as μ, initial Pb isotope ratios, and time, make the Pb isotope system a robust tool for modelling mixing and evolution models of mantle components.

Pb isotopic evolution of the earth has been modelled by various researchers in order to explain the present day crustal and mantle isotope ratios (Stacey and Kramers, 1975; Rudnick *et al.*, 1990; Kamber *et al.*, 2003; Kelley *et al.*, 2005; Halliday, 2008; Connelly and Bizzarro, 2016; Maltese and Mezger, 2020; Fang *et al.*, 2022; Hartnady *et al.*, 2022; Liu *et al.*, 2022). Stacey and Kramers (1975) developed the two-stage evolution model from a primordial Pb isotope ratio of the solar system (equivalent to the Canyon Diablo troilite) for the bulk silicate Earth (BSE) which suggests a change in $^{238}U/^{204}Pb$ ratio (denoted as μ) at ~3.7 Ga to reach the present day "average lead" or BSE Pb isotope ratios. As the geological evolution of the earth does not provide an explanation for the change in μ from 7.19 to 9.74 at 3.7 Ga, required to reach present day BSE, alternate models (e.g., Maltese and Mezger, 2020) have been proposed for the evolution of the BSE. Maltese and Mezger (2020) modelled Pb isotopic evolution of the BSE by assuming a volatile depleted proto-Earth (μ = 100) and a chondritic Theia (μ = 0.188) colliding to produce the Earth-Moon system. Recently reported Pb isotope ratios from Paleoarchean to Neoarchean feldspar grains from Pilbara Craton (Hartnady *et al.*, 2022) conform to the Maltese and Mezger (2020) model. We use the model proposed by Maltese and Mezger (2020) as the starting point to develop the LOMU signature of East Asia. Assuming that the LOMU signature is generated from ancient, subducted sediments (Eisele *et al.*, 2002; Wang *et al.*, 2017), these sediments are likely to have shown similar Pb isotopic ratios to the upper continental crust (UCC) at the time of subduction. So, first we determine the Pb isotopic evolution of the average UCC which has fractionated from the BSE. Although the UCC has been generated and accumulated in phases since 4.3 Ga (Condie, 2021; Hartnady *et al.*, 2022), we assume that the present day average UCC (Millot *et al.*, 2004) can be backtracked to calculate the Pb isotopic ratios of the average UCC at any previous point of time. Theline connecting present-day BSE and the average UCC defines an isochrone on $^{206}Pb/^{204}Pb$ vs $^{207}Pb/^{204}Pb$ diagram (Fig. 8a) which intersects the BSE curve at 2.6 Ga which is taken to be a model age of the average UCC. Initial $^{206}Pb/^{204}Pb$, $^{207}Pb/^{204}Pb$ and $^{208}Pb/^{204}Pb$ ratios are taken from the BSE curve at 2.6 Ga. μ and κ are selected to satisfy the equations:

$$\left(\frac{^{206}Pb}{^{204}Pb}\right)_{t_0} = \left(\frac{^{206}Pb}{^{204}Pb}\right)_{t_1} + \mu\left(e^{\lambda_{238}t_1} - 1\right)\ldots\ldots\ldots\ldots\ldots\ldots\ldots\ldots\ldots\ldots (1)$$

$$\left(\frac{^{207}Pb}{^{204}Pb}\right)_{t_0} = \left(\frac{^{207}Pb}{^{204}Pb}\right)_{t_1} + \frac{\mu}{137.818}\left(e^{\lambda_{235}t_1} - 1\right)\ldots\ldots\ldots\ldots\ldots\ldots\ldots\ldots (2)$$

$$\left(\frac{^{208}Pb}{^{204}Pb}\right)_{t_0} = \left(\frac{^{208}Pb}{^{204}Pb}\right)_{t_1} + \mu \cdot \kappa\left(e^{\lambda_{232}t_1} - 1\right)\text{.........................(3)}$$

Where $\left(\frac{^{20x}Pb}{^{204}Pb}\right)_{t_0}$ is the Pb isotopic ratio at present; $\left(\frac{^{20x}Pb}{^{204}Pb}\right)_{t_1}$ is the Pb isotopic ratio at time t_1; λ_{238}, λ_{235} and λ_{232} are the decay constants for ^{238}U, ^{235}U and ^{232}Th; μ is $^{238}U/^{204}Pb$ at present time and κ is $^{232}Th/^{238}U$ at present time. The Pb isotopic evolution curve for UCC is plotted by forward modelling in 100 million years steps, from the initial Pb isotope ratios at 2.6 Ga, and μ and κ of 10.6 and 4.05 respectively (Fig. 8).

The linear trend shown by Xiaogulihe ultrapotassic rocks (Sun *et al.*, 2014) in Pb isotopic diagrams, is at a steep angle to the BSE and UCC curves and cannot be explained by evolution of a single source with variable μ as suggested by Wang et al. (2017). It is more likely that the trend represents mixing between two different components. Hance, at least two sources are needed to explain the evolution of the two LOMU components. Isochrones connecting the present-day average UCC and the endmembers for the Xiaogulihe-trend intersect the UCC curve at 1.8 and 2.2 Ga which are taken to be the ages of subduction for the two LOMU sources (Fig. 8b). These sources are then evolved with μ and κ of 2.8 and 4.75 for the 1.8 Ga source and 4.26 and 4.0 for the 2.2 Ga source. The μ and κ are selected so to match the isotopic ratios at ends of the Xiaogulihe linear trend. The East Asia low μ samples can now be explained by mixing between the two LOMU sources with the SCLM, as the Pb isotopic ratios from SCLM xenoliths of Korea reported by Choi *et al.* (2005) lie on the linear trend connecting the LOMU members from northeast China and Southwest Japan (Fig. 8).

The ages of subduction agree to repeated subduction and collision models for the North China Craton during the Paleoproterozoic (Santosh, 2010; Wang *et al.*, 2010; Zhao *et al.*, 2012b) which suggests that repeated subduction of sediments are likely to have taken place which may have accumulated near the mantle transition zone below the Archean North

China Craton. Dehydration from the stagnant Pacific slab samples material from the deep asthenospheric mantle metasomatized by the ancient, subducted sediments. It is likely that the metasomatized asthenospheric mantle upwells due to hydration from the stagnant Pacific plate and produces primary melt near the lithosphere asthenosphere boundary (Sakuyama *et al.*, 2014b, 2014a; Kuritani *et al.*, 2017). A schematic diagram representing the tectonic model is presented in Fig. 9.

CONCLUSION

This study establishes the presence of a LOMU type mantle component, in the hydrous asthenospheric mantle, below the northern Kyushu area of southwest Japan. The alkali basalts generated by melting of the shallow asthenospheric to deep lithospheric mantle at ~ 3 Ma, show an isotopic mixing trend between LOMU type components residing in the asthenospheric mantle, and material from the subcontinental lithospheric mantle. However, older (~6 - 8 Ma) alkali basalts about 30 km southeast of this area do not show a LOMU signature. Enrichment in fluid mobile elements inversely correlated to Pb isotopic ratios in the Higashi-Matsuura basalts suggests that the asthenospheric mantle may be metasomatized by melt/fluid derived from ancient, subducted sediments. Recent fluid influx from the stagnant Pacific slab is likely to have triggered melting in the metasomatized asthenospheric mantle producing the East Asian low μ basalts.

The variation visible in the Pb isotope ratios of East Asian LOMU basalts is not consistent with a single Paleoproterozoic subducted sediment component. A Pb isotope evolution model was generated which suggests sediments from two different subduction systems at 2.2 and 1.8 Ga are able to explain the variation observed in the East Asian LOMU basalts.

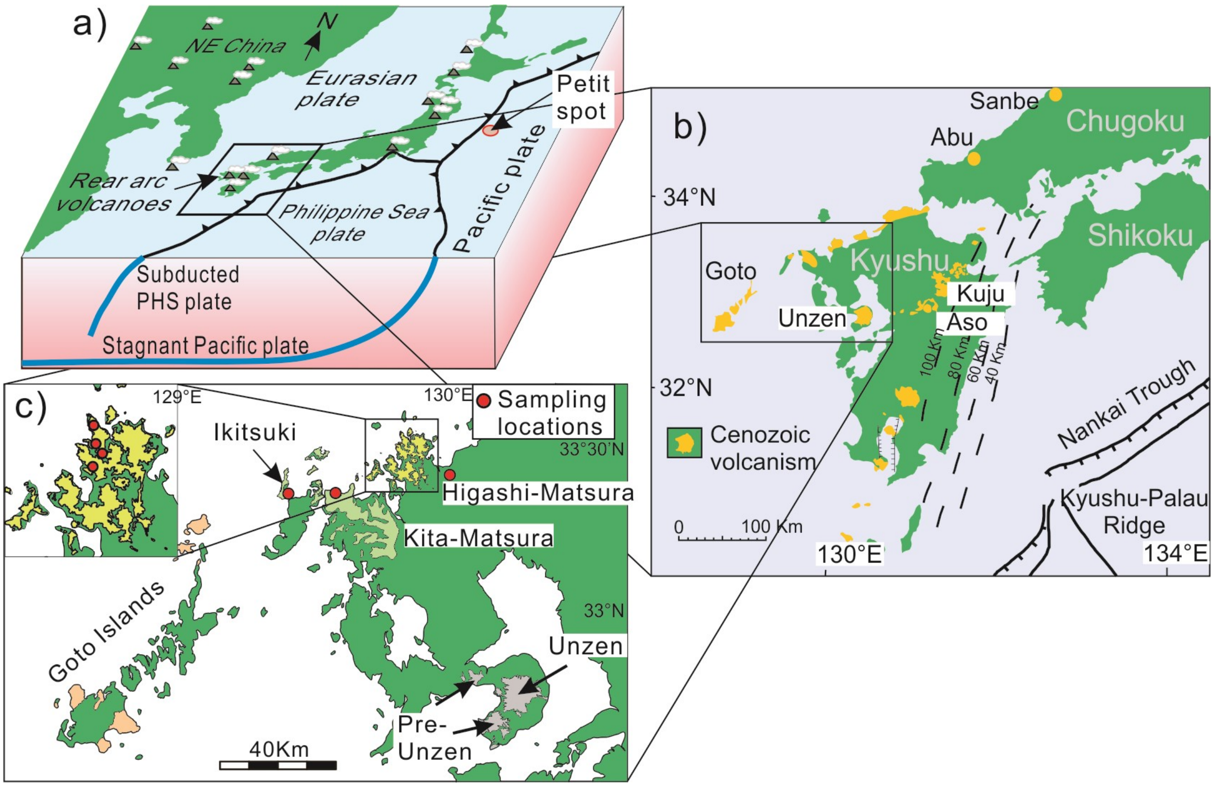

Fig. 1. (a) Schematic diagram of the present-day tectonic setting in East Asia. The subducted Pacific plate is stagnated at the mantle transition zone below East Asia. (b) Location of southwest Japan arc and rear-arc volcanoes. Depth contour for the subducted PHS plate is shown as dashed lines. (c) Cenozoic volcanic fields are differentiated by colour, for rear-arc volcanism in western Kyushu. Sampling locations in Kita-Matsuura and Higashi-Matsuura are indicated by red circles. Locations in Higashi-Matsuura are shown in inset, GPS coordinates are given in Table 1.

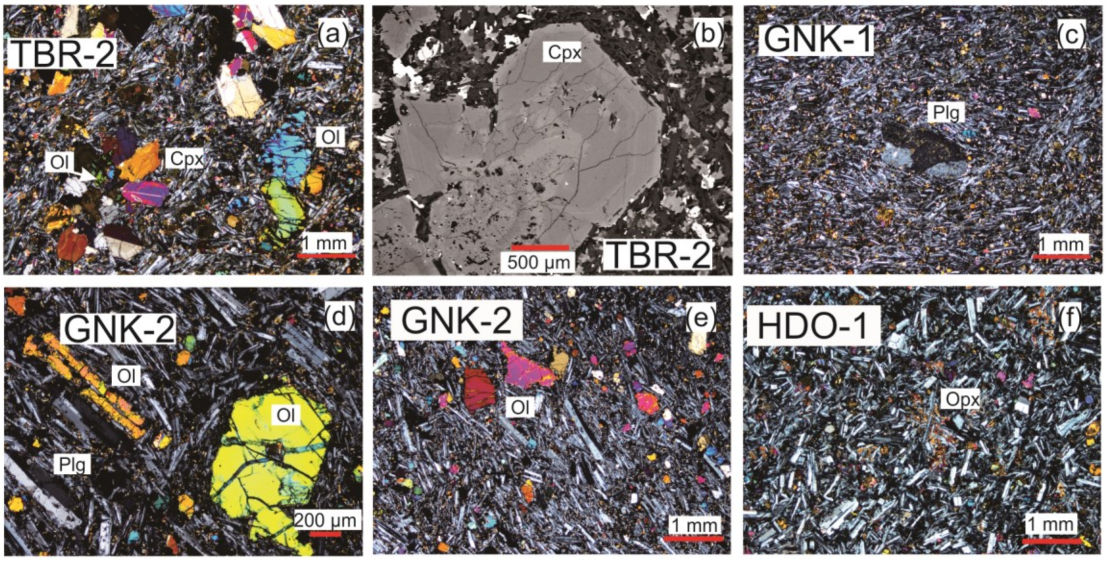

Fig 2. Representative thin sections of alkali basalts from Kita-Matsuura and Higashi-Matsuura. (a) Basalt from Kita-Matsuura (TBR-2) showing clustered clinopyroxene around olivine phenocrysts in plagioclase and orthopyroxene bearing groundmass. Olivine shows normal zoning identifiable by change in birefringence (b) Large clinopyroxene grain (TBR-2) showing compositional zoning in BSE (SEM). (c) Large (1.5 mm) plagioclase phenocryst in fine plagioclase and orthopyroxene bearing groundmass in sample (GNK-1) from Higashi-Matsuura (d) Euhedral and elongate olivine phenocrysts along with plagioclase microphenocrysts in sample (GNK-2) from Higashi-Matsuura. (e) Homogeneous olivine and plagioclase microphenocrysts in plagioclase dominant groundmass visible in Higashi-Matsuura basalt. (f) Randomly oriented plagioclase laths and intergranular orthopyroxene seen in Higashi-Matsuura sample.

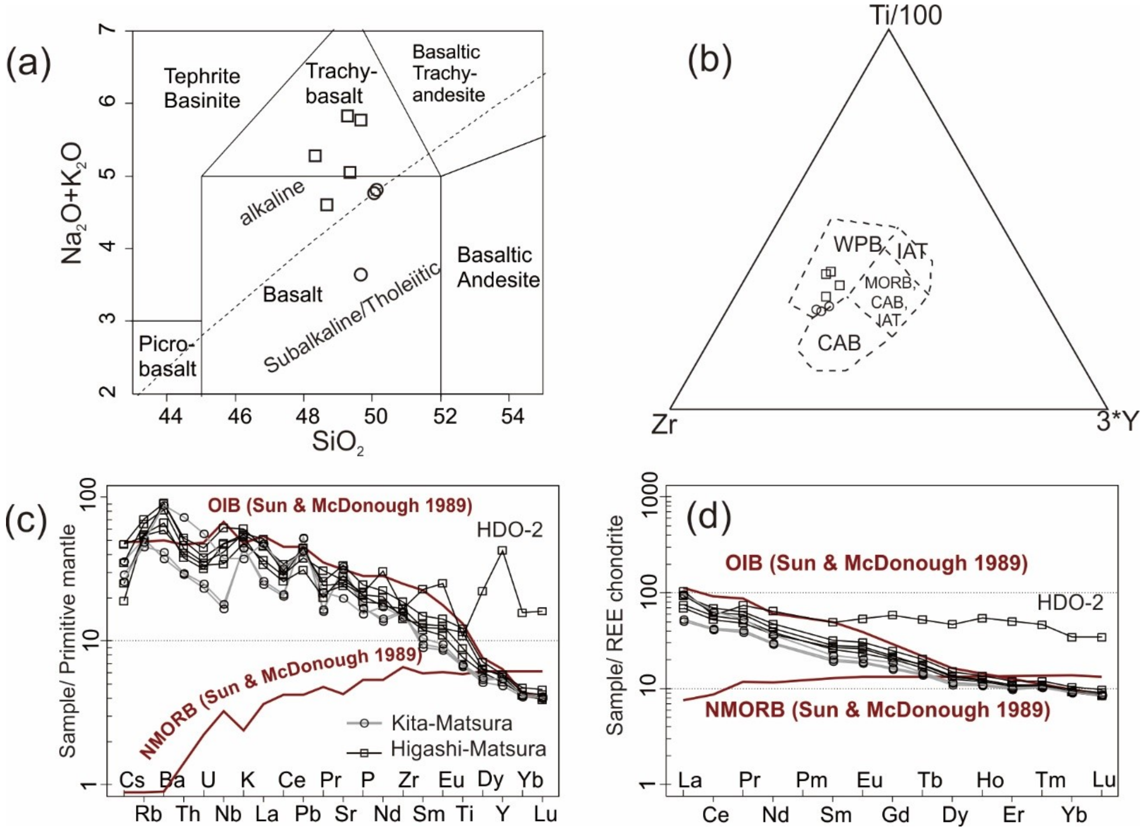

Fig. 3. (a) Total alkali vs. silica diagram (La Bas et al 1986) for the measured samples. Circles and squares represent Kita-Matsuura and Higashi-Matsuura samples respectively. Kita-Matsuura basalts plot in the tholeiitic to alkaline basalt field whereas Higashi-Matsuura samples plot in the alkaline basalt to trachy-basalt field. (b) Geotectonic classification of the analysed samples is plotted according to Pearce and Cann (1973). All samples belong to the within plate basalt group. One sample (HDO-2) has been excluded from this classification for having high Y/Nb ratio. (c) Primitive mantle normalized trace element pattern showing OIB like pattern for measured samples with minor Nb depletion for Kita-Matsuura samples and no depletion for Higashi-Matsuura samples. Fluid mobile elements (Ba, K, Sr, Pb) show enriched signature. HDO-2 shows anomalously high HREE and Y abundance compared to the other samples. (d) Chondrite normalized trace element pattern showing enrichment in LREE compared to HREE with no prominent Eu anomaly.

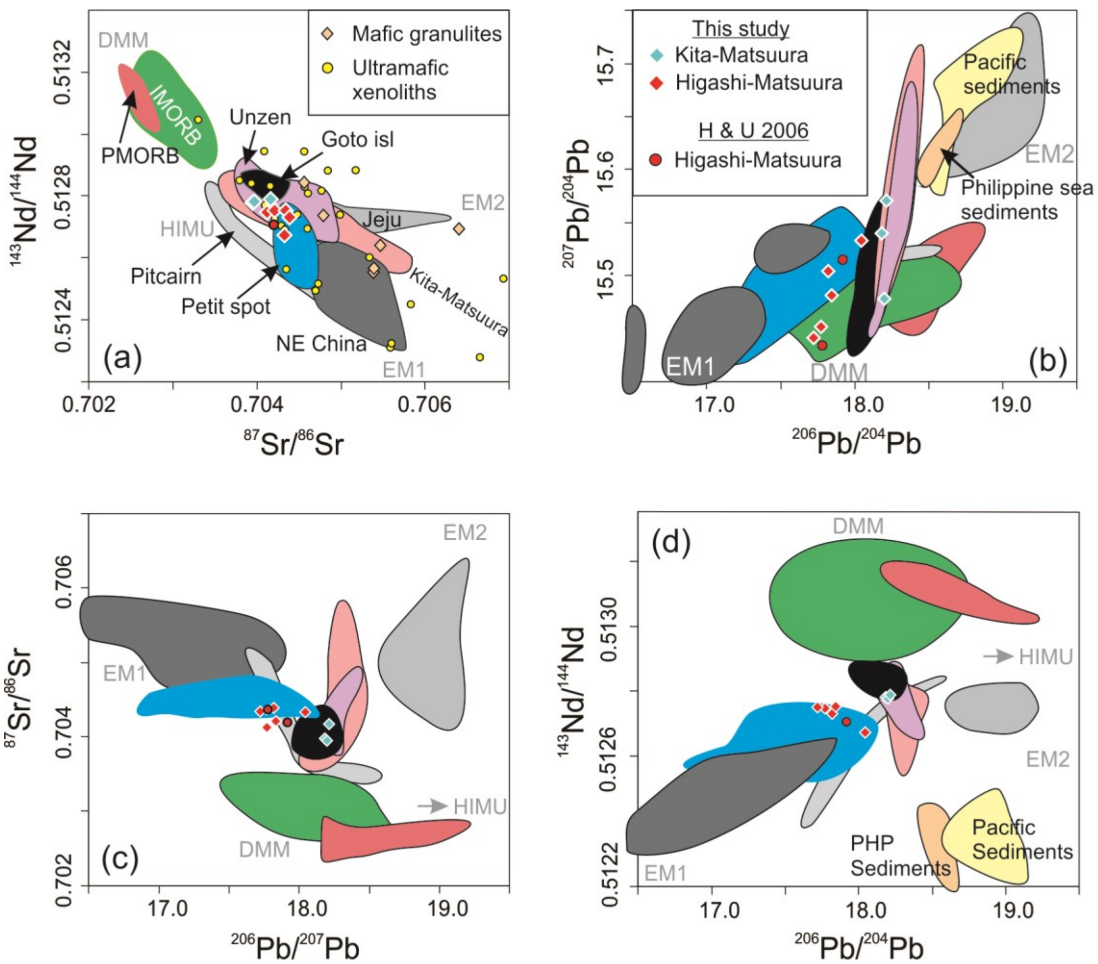

Fig. 4. $^{87}Sr/^{86}Sr$, $^{143}Nd/^{144}Nd$, $^{206}Pb/^{204}Pb$, $^{207}Pb/^{204}Pb$ and $^{208}Pb/^{204}Pb$ ratios of measured samples compared to data from rear arc basalts of Kyushu, i.e., Goto island (Hoang *et al.*, 2013; Kuritani *et al.*, 2017), Unzen (Hoang and Uto, 2006; Sugimoto *et al.*, 2006), Kita-Matsuura (Uto *et al.*, 2004; Sakuyama *et al.*, 2014b). and other components, i.e., northeast China intraplate basalts (Kuritani *et al.*, 2009; Sun *et al.*, 2014; Wang *et al.*, 2017), Jeju (Kim *et al.*, 2019), Pitcairn (Wang *et al.*, 2018), Petit spot (Liu *et al.*, 2020), Indian and Pacific type MORB (Gale *et al.*, 2013) and subducting sediments (Cousens *et al.*, 1994; Saitoh *et al.*, 2015). Sr-Nd data for mantle lower crustal xenoliths show EM 1 and EM 2 like characteristics (Kagami *et al.*, 1993; Ikeda *et al.*, 2001; Senda *et al.*, 2007; Yoshikawa *et al.*, 2010). Two samples from Higashi-Matsuura reported by Hoang and Uto (2006) are shown as red circles.

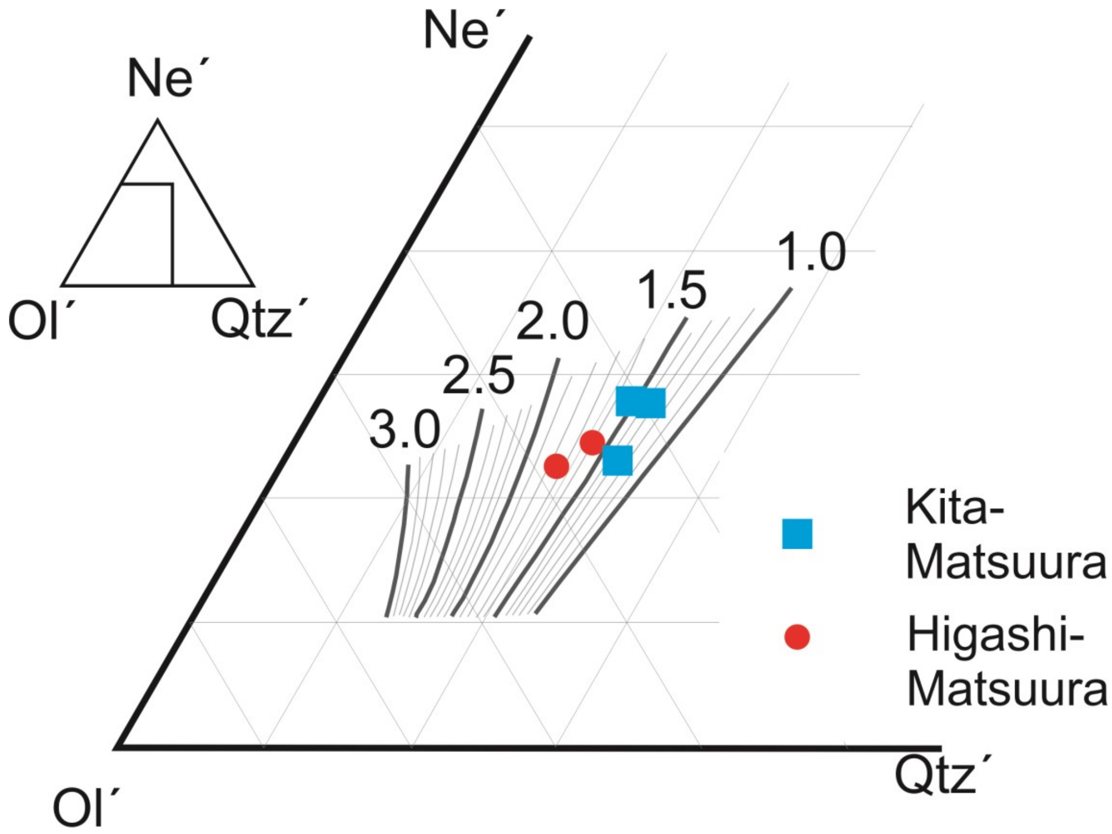

Fig. 5. Ne′-Ol′-Qtz′ plot of normative components from calculated primary magma compositions. Projection scheme from Irvine and Baragar (1971), Ne′ = Ne + 0.6Ab; Qtz′ = Qtz + 0.4Ab + 0.25Opx; Ol′ = Ol + 0.75Opx. Sub-vertical lines from 1.0- 3.0 represent isopleths of melting pressure (GPa) after Sakuyama et al. (2009).

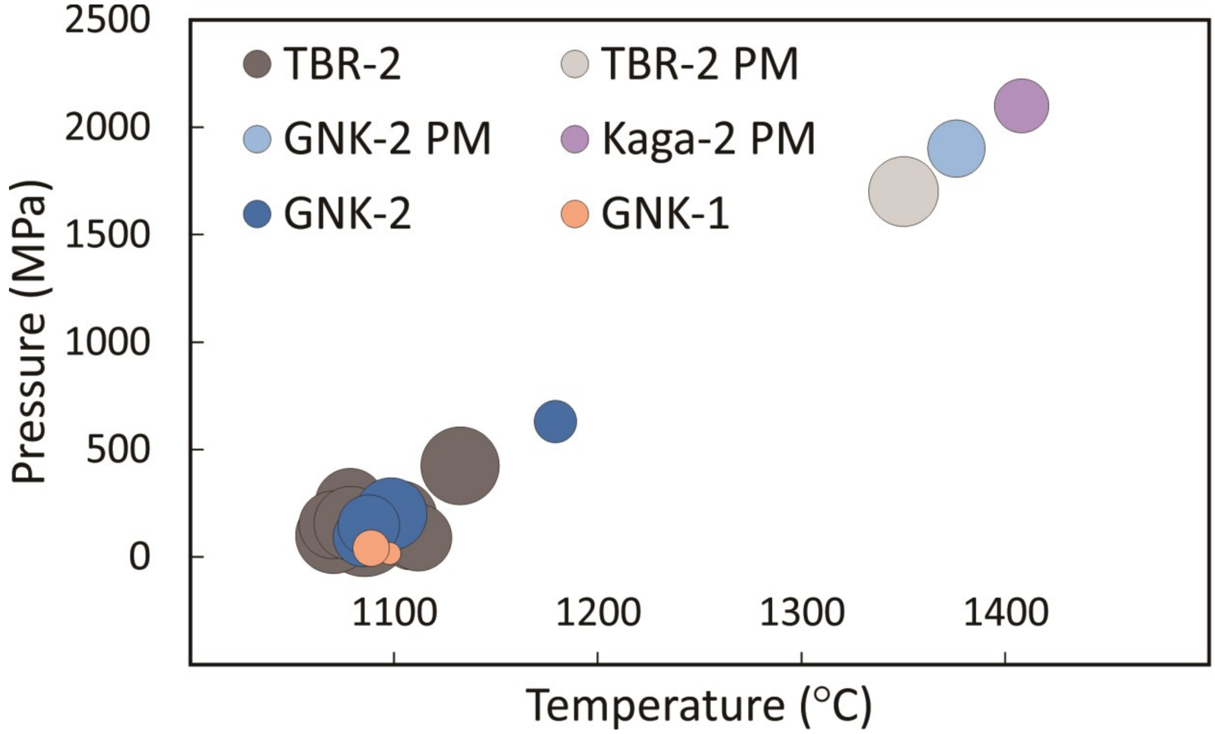

Fig. 6. Pressure vs. temperature plot for Higashi-Matsuura (GNK-1, GNK-2, Kaga-2) and Kita-Matsuura (TBR-2). PM samples represent primary magma and pressure and temperature of mantle melting. Other data points refer to pressure and temperature of Cpx crystallization after olivine fractionation. Diameter of circles represents relative H_2O content in the primary magma or equilibrium magma during Cpx crystallization.

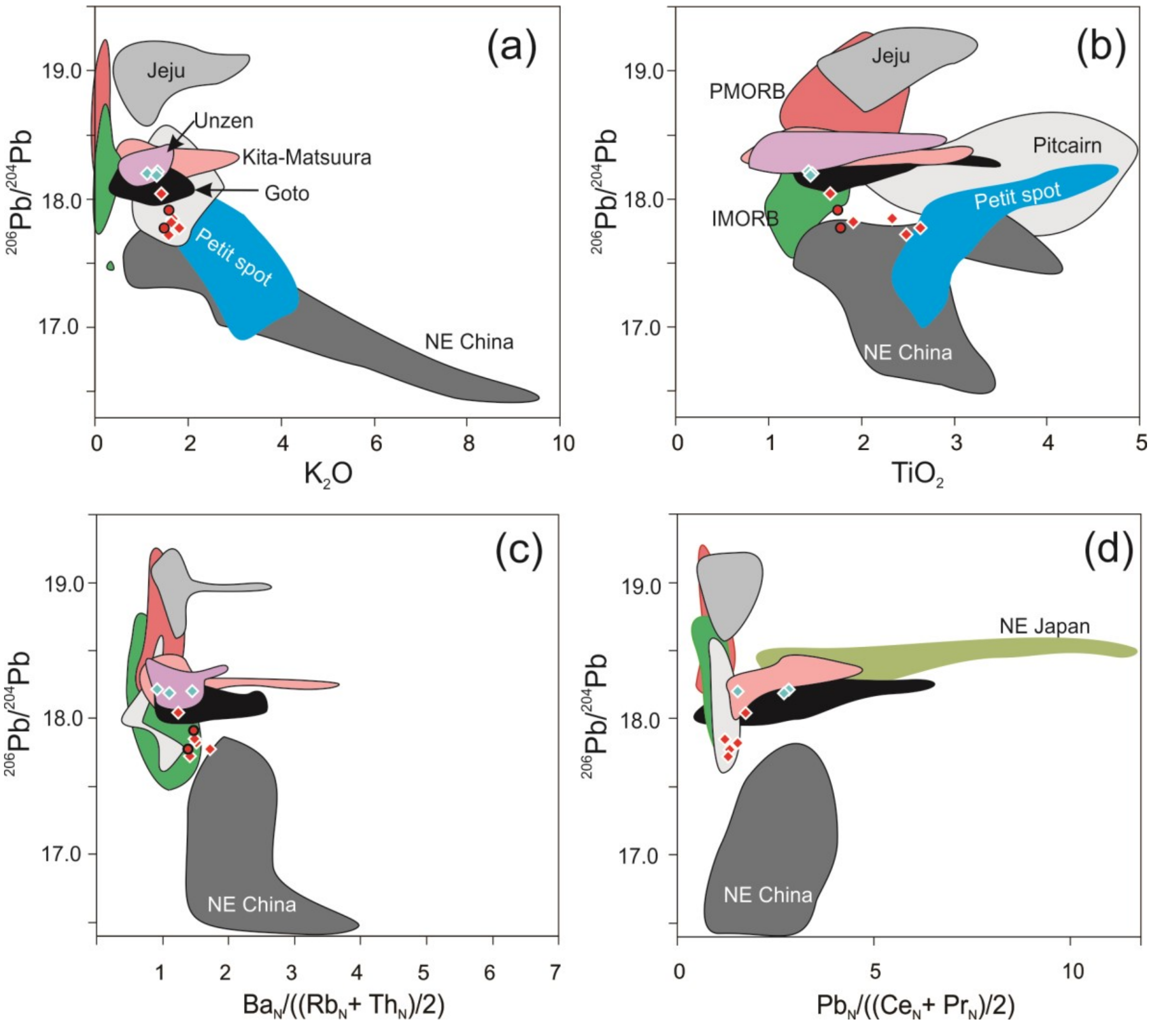

Fig. 7. Correlation of (a) K2O, (b) TiO2, (c) Ba and (d) Pb with respect to $^{206}Pb/^{204}Pb$ ratio. Ba and Pb is plotted as enrichment over expected values from adjacent elements in primitive mantle normalized trace element patterns. Similar trend to Higashi-Matsuura is seen for northeast China intraplate basalts. Petit spot basalts show similar trend for K_2O but an inverse trend for TiO_2. Colour and symbols are same as Fig. 4.

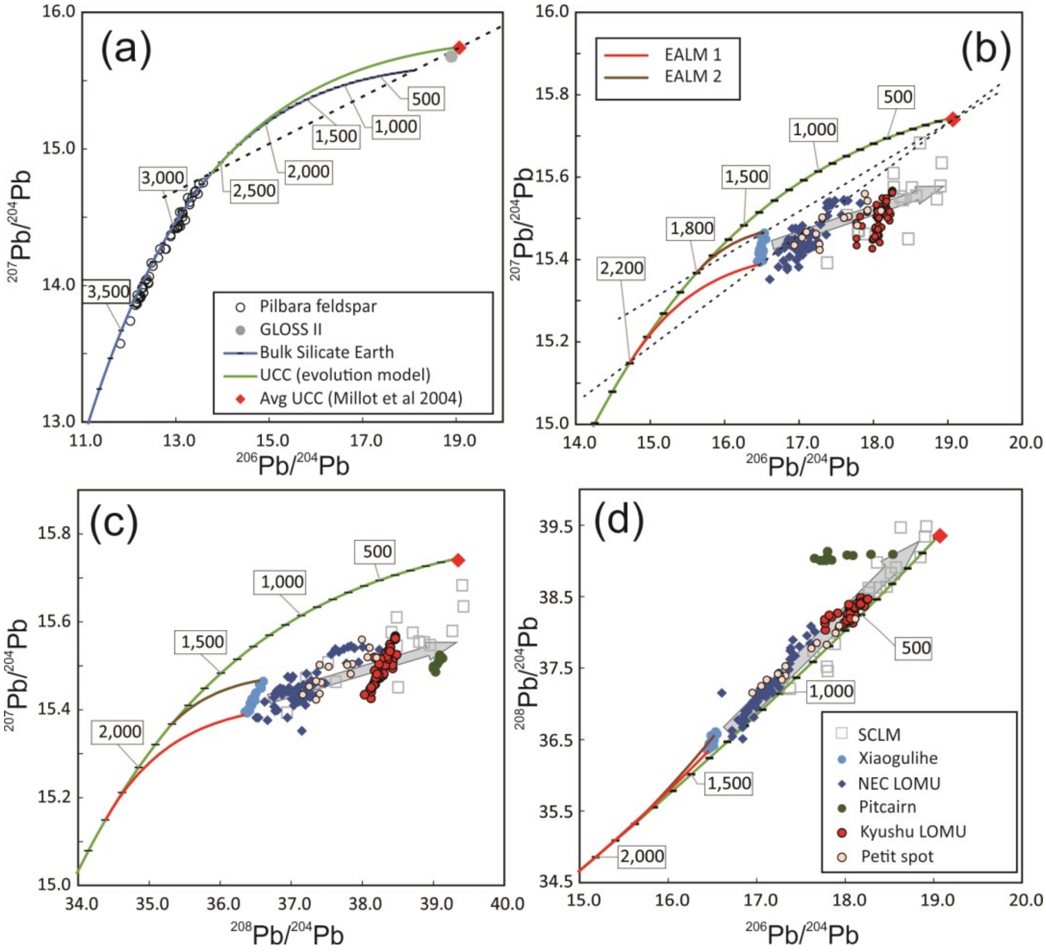

Fig. 8. Pb isotopic evolution model and mixing model for East Asian Low μ (EALM) basalts. Numbers in boxes represent age in Ma. (a) Evolution model for Bulk silicate Earth (BSE) and average upper continental crust (UCC). BSE model is taken from Maltese and Mezger (2020). Pb isotopic ratios of Archean feldspars from Pilbara craton are taken from Hartnady et al. (2022). UCC evolution model is calculated using average composition from Millot et al. (2004) and corresponding μ and κ of 10.6 and 4.05 respectively for a time of fractionation of 2.6 Ga (See text for details). Pb isotope ratio for global subducting sediments (GLOSS-II; Plank 2014) plots near the estimate for average UCC and falls on the isochron for UCC. (b) Model evolution for two low μ end members (EALM-1 and EALM-2) for Xiaogulihe ultrapotassic rocks. Model age for these two subducting sediment components were estimated to be 2.2 and 1.8 Ga. Corresponding μ were calculated as 4.26 and 2.8 respectively. (c) and (d) shows same components w.r.t $^{208}Pb/^{204}Pb$. κ for EALM-1 and EALM-2 were calculated as 4.0 and 4.75 respectively. Pb isotopic data from EM 1 type area Pitcairn do not fall on the same trend as East Asian low μ basalts. Pb isotopic data for Xiaogulihe is from Sun et al. (2014) Other samples from northeast China (Wudalianchi, Nuominhe, Erkeshan, Keluo, Changbaishan) are from Wang et al. (2017) and references therein, and Kuritani et al. (2009); Petit spot basalts are from Liu et al. (2020); Kyushu low μ basalts are from this study and Hoang et al. 2013 and Kuritani et al. 2017. Data from subcontinental lithospheric mantle (SCLM) xenoliths are from Choi et al. (2005).

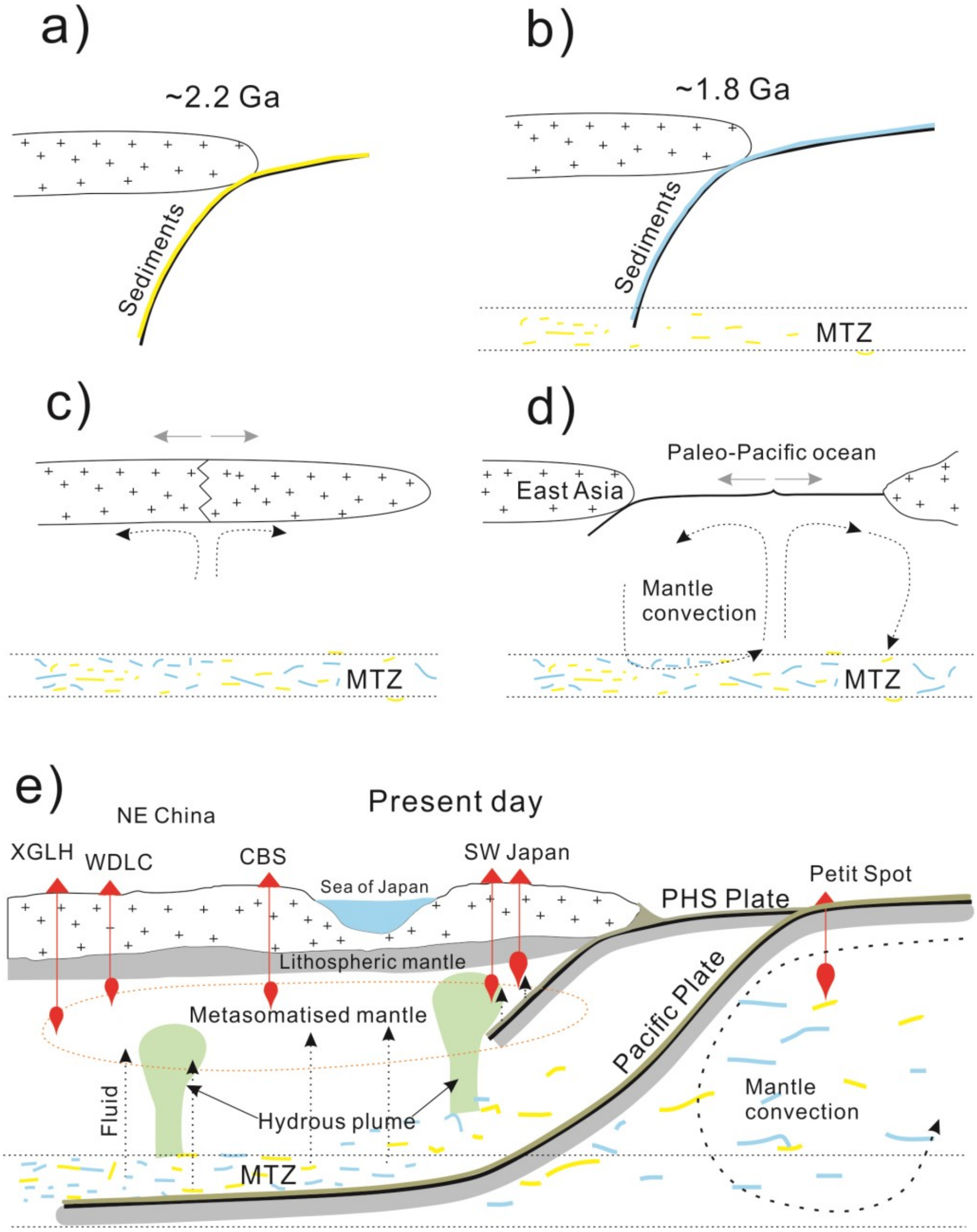

Fig. 9. Schematic diagram representing the evolution of the East Asian low μ component. (a) to (e) represents change in tectonic setting through time. Two different subduction events contributed sediments which are accumulated at the mantle transition zone and evolve with a low U/Pb ratio up to present time. The two sediment components are assumed to have retained their individual geochemical traits without being homogenized as a single domain. Fluid induced upwelling and melting of the metasomatized mantle generate the low radiogenic Pb bearing alkali basalts.

Bibliography

Basu, A. R., Wang Junwen, Huang Wankang, Xie Guanghong & Tatsumoto, M. (1991). Major element, REE, and Pb, Nd and Sr isotopic geochemistry of Cenozoic volcanic rocks of eastern China: implications for their origin from suboceanic-type mantle reservoirs. *Earth and Planetary Science Letters*. Elsevier **105**, 149–169.

Birck, J. L. (1986). Precision K□Rb□Sr isotopic analysis: Application to Rb□Sr chronology. *Chemical Geology* **56**, 73–83.

Chang, Q., Shibata, T., Shinotsuka, K., Yoshikawa, M. & Tatsumi, Y. (2002). Precise determination of trace elements in geological standard rocks using inductively coupled plasma mass spectrometry (ICP-MS). *Frontier Research on Earth Evolution* **1**, 357–362.

Chen, H., Xia, Q.-K., Ingrin, J., Jia, Z.-B. & Feng, M. (2015). Changing recycled oceanic components in the mantle source of the Shuangliao Cenozoic basalts, NE China: New constraints from water content. *Tectonophysics*. Elsevier **650**, 113–123.

Chen, H., Xia, Q.-K. K., Ingrin, J., Deloule, E. & Bi, Y. (2017). Heterogeneous source components of intraplate basalts from NE China induced by the ongoing Pacific slab subduction. *Earth and Planetary Science Letters*. Elsevier **459**, 208–220.

Chen, Y., Zhang, Y., Graham, D., Su, S. & Deng, J. (2007). Geochemistry of Cenozoic basalts and mantle xenoliths in Northeast China. *Lithos*. Elsevier **96**, 108–126.

Choi, H. O., Choi, S. H., Lee, Y. S., Ryu, J. S., Lee, D. C., Lee, S. G., Sohn, Y. K. & Liu, J. qi (2020). Petrogenesis and mantle source characteristics of the late Cenozoic Baekdusan (Changbaishan) basalts, North China Craton. *Gondwana Research*. Elsevier Ltd **78**, 156–171.

Choi, S. H., Kwon, S.-T., Mukasa, S. B. & Sagong, H. (2005). Sr–Nd–Pb isotope and trace element systematics of mantle xenoliths from Late Cenozoic alkaline lavas, South Korea. *Chemical Geology*. Elsevier **221**, 40–64.

Choi, S. H. & Liu, S.-A. (2022). Zinc isotopic systematics of the Mt. Baekdu and Jeju Island intraplate basalts in Korea, and implications for mantle source lithologies. *Lithos* **416–417**, 106659.

Choi, S. H., Mukasa, S. B., Kwon, S. T. & Andronikov, A. V. (2006). Sr, Nd, Pb and Hf isotopic compositions of late Cenozoic alkali basalts in South Korea: Evidence for mixing between the two dominant asthenospheric mantle domains beneath East Asia. *Chemical Geology* **232**, 134–151.

Compston, W. & Oversby, V. M. (1969). Lead Isotopic Analysis Using a Double Spike. *Journal of Geophysical Research*. Wiley-Blackwell **74**, 4338–4348.

Condie, K. C. (2021). *Earth as an Evolving Planetary System*. *Elsevier*. Elsevier.

Connelly, J. N. & Bizzarro, M. (2016). Lead isotope evidence for a young formation age of the Earth–Moon system. *Earth and Planetary Science Letters*. Elsevier B.V. **452**, 36–43.

Cooper, L. B. *et al.* (2012). Global variations in H2O/Ce: 1. Slab surface temperatures beneath volcanic arcs. *Geochemistry, Geophysics, Geosystems*. John Wiley & Sons, Ltd **13**.

Depaolo, D. J. (1988). *Neodymium Isotope Geochemistry: an introduction*. *Springer-Verlag*.

DePaolo, D. J. (1981). Trace element and isotopic effects of combined wallrock assimilation and fractional crystallization. *Earth and Planetary Science Letters*. Elsevier **53**, 189–202.

Dey, B., Shibata, T. & Yoshikawa, M. (2023). Sequential Pb-Sr-LREE separation from silicates for isotopic analysis. *Geochemical Journal* **57**, 73–84.

Eisele, J., Sharma, M., Galer, S. J. G. G., Blichert-Toft, J., Devey, C. W. & Hofmann, A. W. (2002). The role of sediment recycling in EM-1 inferred from Os, Pb, Hf, Nd, Sr isotope and trace element systematics of the Pitcairn hotspot. *Earth and Planetary Science Letters*. Elsevier **196**, 197–212.

Fang, T., Huang, J. & Zartman, R. E. (2022). Lead isotope evolution during the multi-stage core formation. *Solid Earth Sciences*. Guangzhou Institute of Geochemistry **7**, 50–59.

Fukao, Y., Obayashi, M., Inoue, H. & Nenbai, M. (1992). Subducting slabs stagnant in the mantle transition zone. *Journal of Geophysical Research* **97**, 4809–4822.

Ghiorso, M. S., Hirschmann, M. M., Reiners, P. W. & Kress, V. C. (2002). The pMELTS: A revision of MELTS for improved calculation of phase relations and major element partitioning related to partial melting of the mantle to 3 GPa. *Geochemistry, Geophysics, Geosystems* **3**, 1–35.

Halliday, A. N. (2008). A young Moon-forming giant impact at 70 – 110 million years accompanied by late-stage mixing , core formation and degassing of the Earth. *Philosophical Transactions of the Royal Society A* **366**, 4163–4181.

Hartnady, M. I. H., Kirkland, C. L., Smithies, R. H., Johnson, S. P. & Johnson, T. E. (2022). Pb isotope insight into the formation of the Earth's first stable continents. *Earth and Planetary Science Letters*. Elsevier B.V. **578**, 117319.

Herzberg, C. & O'hara, M. J. (2002). *Plume-Associated Ultramafic Magmas of Phanerozoic Age*. *JOURNAL OF PETROLOGY*.

Hirano, N. & Machida, S. (2022). The mantle structure below petit-spot volcanoes. *Communications Earth and Environment*. Springer US **3**, 1–11.

Hirschmann, M. M. (2006). WATER, MELTING, AND THE DEEP EARTH H2O CYCLE. *Annual Review of Earth and Planetary Sciences*. Annual Reviews **34**, 629–653.

Hoang, N. & Uto, K. (2003). Geochemistry of Cenozoic basalts in the Fukuoka district (northern Kyushu, Japan): Implications for asthenosphere and lithospheric mantle interaction. *Chemical Geology* **198**, 249–268.

Hoang, N. & Uto, K. (2006). Upper mantle isotopic components beneath the Ryukyu arc system: Evidence for "back-arc" entrapment of Pacific MORB mantle. *Earth and Planetary Science Letters*. Elsevier **249**, 229–240.

Hoang, N., Uto, K., Matsumoto, A. & Itoh, J. (2013). Pleistocene intraplate magmatism in the Goto Islands, SW Japan: Implications for mantle source evolution and regional geodynamics. *Journal of Geodynamics*. Pergamon **68**, 1–17.

Huang, Z., Zhao, D., Hasegawa, A., Umino, N., Park, J. H. & Kang, I. B. (2013). Aseismic deep subduction of the Philippine Sea plate and slab window. *Journal of Asian Earth Sciences* **75**, 82–94.

Ikeda, Y., Nagao, K. & Kagami, H. (2001). Effects of recycled materials involved in a mantle source beneath the southwest Japan arc region: evidence from noble gas, Sr, and Nd isotopic systematics. *Chemical Geology* **175**, 509–522.

Irvine, T. N. & Baragar, W. R. A. (1971). A Guide to the Chemical Classification of the Common Volcanic Rocks. *Canadian Journal of Earth Sciences* **8**, 523–548.

Kagami, H., Iwata, M., Iizumi, S. & Nureki, T. (1993). Sr-Nd Isotope Systematics of Xenoliths in Cenozoic Volcanic Rocks from SW Japan. *Proceedings of the Japan Academy, Series B* **69**, 1–6.

Kamata, H. & Kodama, K. (1999). Volcanic history and tectonics of the Southwest Japan Arc. *The Island Arc*. Wiley/Blackwell (10.1111) **8**, 393–403.

Kamber, B. S., Collerson, K. D., Moorbath, S. & Whitehouse, M. J. (2003). Inheritance of early archaean Pb-isotope variability from long-lived hadean protocrust. *Contributions to Mineralogy and Petrology* **145**, 25–46.

Kanazawa, T., Sager, W. & Escutia, C. (2001). Explanatory Notes. *Proceedings of the Ocean Drilling Program, Initial Reports Volume 191*, 46.

Kelley, K. A., Plank, T., Farr, L., Ludden, J. & Staudigel, H. (2005). Subduction cycling of U , Th , and Pb. *Earth and Planetary Science Letters* **234**, 369–383.

Kelley, K. A., Plank, T., Grove, T. L., Stolper, E. M., Newman, S. & Hauri, E. (2006). Mantle melting as a function of water content beneath back-arc basins. *Journal of Geophysical Research: Solid Earth*. John Wiley & Sons, Ltd **111**, 9208.

Kuritani, T., Kimura, J.-I., Miyamoto, T., Wei, H., Shimano, T., Maeno, F., Jin, X. & Taniguchi, H. (2009). Intraplate magmatism related to deceleration of upwelling asthenospheric mantle: Implications from the Changbaishan shield basalts, northeast China. *Lithos*. Elsevier **112**, 247–258.

Kuritani, T., Kimura, J.-I., Ohtani, E., Miyamoto, H. & Furuyama, K. (2013). Transition zone origin of potassic basalts from Wudalianchi volcano, northeast China. *Lithos*. Elsevier **156–159**, 1–12.

Kuritani, T., Ohtani, E. & Kimura, J. (2011). Intensive hydration of the mantle transition zone beneath China caused by ancient slab stagnation. *Nature Geoscience*. Nature Publishing Group **4**, 713–716.

Kuritani, T., Sakuyama, T., Kamada, N., Yokoyama, T. & Nakagawa, M. (2017). Fluid-fluxed melting of mantle versus decompression melting of hydrous mantle plume as the cause of intraplate magmatism over a stagnant slab: Implications from Fukue Volcano Group, SW Japan. *Lithos* **282–283**, 98–110.

Kuritani, T., Xia, Q.-K. Q.-K., Kimura, J.-I. J.-I., Liu, J., Shimizu, K., Ushikubo, T., Zhao, D., Nakagawa, M. & Yoshimura, S. (2019). Buoyant hydrous mantle plume from the mantle transition zone. *Scientific Reports*. Nature Publishing Group **9**, 6549.

Le Bas, M. J., Le Maitre, R. W., Streckeisen, A. & Zanettin, B. (1986). A chemical classification of volcanic rocks based on the total alkali-silica diagram. *Journal of Petrology*. Oxford Academic **27**, 745–750.

Li, S. G. *et al.* (2017). Deep carbon cycles constrained by a large-scale mantle Mg isotope anomaly in eastern China. *National Science Review* **4**, 111–120.

Li, T. (2010). The principal characteristics of the lithosphere of China. *Geoscience Frontiers*. Elsevier **1**, 45–56.

Liu, D., Guo, J., Jiang, N., Hu, J., Mitchell, R. N., Fan, W., Mao, Q. & Zhao, L. (2022). Lead isotopic compositions of late Archean lower continental crust. *Geochimica et Cosmochimica Acta*. Elsevier Ltd **337**, 95–105.

Liu, J. *et al.* (2020). Melting of recycled ancient crust responsible for the Gutenberg discontinuity. *Nature Communications*. Springer US **11**, 1–9.

Liu, J. Q., Chen, L. H., Wang, X. J., Zhong, Y., Yu, X., Zeng, G. & Erdmann, S. (2017). The role of melt-rock interaction in the formation of Quaternary high-MgO potassic basalt from the Greater Khingan Range, northeast China. *Journal of Geophysical Research: Solid Earth*. John Wiley & Sons, Ltd **122**, 262–280.

Liu, S. A. & Li, S. G. (2019). Tracing the Deep Carbon Cycle Using Metal Stable Isotopes: Opportunities and Challenges. *Engineering*. Chinese Academy of Engineering **5**, 448–457.

Machida, S., Hirano, N. & Kimura, J. I. (2009). Evidence for recycled plate material in Pacific upper mantle unrelated to plumes. *Geochimica et Cosmochimica Acta*. Elsevier Ltd **73**, 3028–3037.

Mahony, S. H., Wallace, L. M., Miyoshi, M., Villamor, P., Sparks, R. J. & Hasenaka, T. (2011). Volcano-tectonic interactions during rapid plate-boundary evolution in the Kyushu region, SW Japan. *Bulletin of the Geological Society of America*.

GeoScienceWorld **123**, 2201–2223.

Maltese, A. & Mezger, K. (2020). The Pb isotope evolution of Bulk Silicate Earth: Constraints from its accretion and early differentiation history. *Geochimica et Cosmochimica Acta*. Elsevier Ltd **271**, 179–193.

Menzies, M. A. (1995). Potassic Volcanic Rocks in NE China : Geochemical Constraints on Mantle Source and Magma Genesis. **36**, 1275–1303.

Michael, P. (1995). Regionally distinctive sources of depleted MORB: Evidence from trace elements and H2O. *Earth and Planetary Science Letters* **131**, 301–320.

Millot, R., Allègre, C.-J. J., Gaillardet, J. & Roy, S. (2004). Lead isotopic systematics of major river sediments: a new estimate of the Pb isotopic composition of the Upper Continental Crust. *Chemical Geology*. Elsevier **203**, 75–90.

Nakamura, E., McDougall, I. & Campbell, I. H. (1986). K-Ar ages of basalts from the Higashi-Matsuura district, northwestern Kyushu, Japan and regional geochronology of the Cenozoic alkaline volcanic rocks in eastern Asia. *GEOCHEMICAL JOURNAL* **20**, 91–99.

Pearce, J. A. & Cann, J. R. (1973). Tectonic setting of basic volcanic rocks determined using trace element analyses. *Earth and Planetary Science Letters* **19**, 290–300.

Pearce, T. H. (1978). Olivine fractionation equations for basaltic and ultrabasic liquids. *Nature* **276**, 771–774.

Perinelli, C., Mollo, S., Gaeta, M., De Cristofaro, S. P., Palladino, D. M., Armienti, P., Scarlato, P. & Putirka, K. D. (2016). An improved clinopyroxene-based hygrometer for Etnean magmas and implications for eruption triggering mechanisms. *American Mineralogist* **101**, 2774–2777.

Putirka, K. D. (2008). Thermometers and barometers for volcanic systems. *Reviews in Mineralogy and Geochemistry* **69**, 61–120.

Richard, G. C. & Iwamori, H. (2010). Stagnant slab, wet plumes and Cenozoic volcanism in East Asia. *Physics of the Earth and Planetary Interiors* **183**, 280–287.

Roeder, P. L. & Emslie, R. F. (1970). Olivine-liquid equilibrium. *Contributions to Mineralogy and Petrology*. Springer-Verlag **29**, 275–289.

Rudnick, R. L., Goldstine, S. L., Goldstein, S. L., Goldstine, S. L., Goldstein, S. L., Goldstine, S. L. & Goldstein, S. L. (1990). The Pb isotopic compositions of lower crustal xenoliths and the evolution of lower crustal Pb. *Earth and Planetary Science Letters* **98**, 192–207.

Sakuyama, T. *et al.* (2013). Melting of dehydrated oceanic crust from the stagnant slab and of the hydrated mantle transition zone: Constraints from Cenozoic alkaline basalts in eastern China. *Chemical Geology*. Elsevier **359**, 32–48.

Sakuyama, T. *et al.* (2014a). Melting of the Uppermost Metasomatized Asthenosphere

Triggered by Fluid Fluxing from Ancient Subducted Sediment: Constraints from the Quaternary Basalt Lavas at Chugaryeong Volcano, Korea. *Journal of Petrology*. Narnia **55**, 499–528.

Sakuyama, T., Nakai, S., Yoshikawa, M., Shibata, T. & Ozawa, K. (2014b). Progressive interaction between dry and wet mantle during high-temperature diapiric upwelling: Constraints from cenozoic kita-matsuura intraplate basalt province, Northwestern Kyushu, Japan. *Journal of Petrology* **55**, 1083–1128.

Sakuyama, T., Ozawa, K., Sumino, H. & Nagao, K. (2009). Progressive melt extraction from upwelling mantle constrained by the kita-matsuura basalts in NW Kyushu, SW Japan. *Journal of Petrology*. Oxford University Press **50**, 725–779.

Salters, V. J. M. & Stracke, A. (2004). Composition of the depleted mantle. *Geochemistry, Geophysics, Geosystems*. Wiley-Blackwell **5**, n/a-n/a.

Santosh, M. (2010). Assembling North China Craton within the Columbia supercontinent: The role of double-sided subduction. *Precambrian Research* **178**, 149–167.

Senda, R., Tanaka, T. & Suzuki, K. (2007). Os, Nd, and Sr isotopic and chemical compositions of ultramafic xenoliths from Kurose, SW Japan: Implications for contribution of slab-derived material to wedge mantle. *Lithos*. Elsevier **95**, 229–242.

Shi, J., Zeng, G., Chen, L., Wang, X., Liu, J., Xie, L., Yang, Y. & Zhang, H. (2023). Lithology of EM1 Reservoir Revealed by Fe Isotopes of Continental Potassic Basalts. *Journal of Geophysical Research: Solid Earth* **128**, 1–17.

Shibata, T., Yoshikawa, M., Itoh, J., Ujike, O., Miyoshi, M. & Takemura, K. (2014). Along-arc geochemical variations in Quaternary magmas of northern Kyushu Island, Japan. *Geological Society, London, Special Publications*. Geological Society of London **385**, 15–29.

Stacey, J. S. & Kramers, J. D. (1975). Approximation of terrestrial lead isotope evolution by a two-stage model. *Earth and Planetary Science Letters* **26**, 207–221.

Sumino, H., Nakai, S. N. I., Nagao, K. & Notsu, K. (2000). High ^{3}He/4He ratio in xenoliths from Takashima: Evidence for plume type volcanism in southwestern Japan. *Geophysical Research Letters*. John Wiley & Sons, Ltd **27**, 1211–1214.

Sun, Y., Teng, F. Z., Ying, J. F., Su, B. X., Hu, Y., Fan, Q. C. & Zhou, X. H. (2017). Magnesium Isotopic Evidence for Ancient Subducted Oceanic Crust in LOMU-Like Potassium-Rich Volcanic Rocks. *Journal of Geophysical Research: Solid Earth*. John Wiley & Sons, Ltd **122**, 7562–7572.

Sun, Y., Ying, J., Zhou, X., Shao, J., Chu, Z. & Su, B. (2014). Geochemistry of ultrapotassic volcanic rocks in Xiaogulihe NE China: Implications for the role of ancient subducted sediments. *Lithos*. Elsevier B.V. **208**, 53–66.

Takai, Y. & Uehara, S. (2012). Rhabdophane-(Y), YPO4·H2O, a new mineral in alkali olivine basalt from Hinodematsu, Genkai-cho, Saga Prefecture, Japan. *Journal of Mineralogical and Petrological Sciences* **107**, 110–113.

Tatsumi, Y., Sakuyama, M., Fukuyama, H. & Kushiro, I. (1983). Generation of arc basalt magmas and thermal structure of the mantle wedge in subduction zones. *Journal of Geophysical Research: Solid Earth*. Wiley-Blackwell **88**, 5815–5825.

Tatsumoto, M. (1969). Lead isotopes in volcanic rocks and possible ocean-floor thrusting beneath island arcs. *Earth and Planetary Science Letters* **6**, 369–376.

Tatsumoto, M. & Nakamura, Y. (1991). DUPAL anomaly in the Sea of Japan: Pb, Nd, and Sr isotopic variations at the eastern Eurasian continental margin. *Geochimica et Cosmochimica Acta*. Pergamon **55**, 3697–3708.

Uto, K., Hoang, N. & Matsui, K. (2004). Cenozoic lithospheric extension induced magmatism in Southwest Japan. *Tectonophysics*. Elsevier **393**, 281–299.

Walter, M. J. (1998). Melting of Garnet Peridotite and the Origin of Komatiite and Depleted Lithosphere. **39**, 29–60.

Wang, X.-J. J., Chen, L.-H. H., Hofmann, A. W. A. W. W., Mao, F.-G. G., Liu, J.-Q. Q., Zhong, Y., Xie, L.-W. W. & Yang, Y.-H. H. (2017). Mantle transition zone-derived EM1 component beneath NE China: Geochemical evidence from Cenozoic potassic basalts. *Earth and Planetary Science Letters*. Elsevier B.V. **465**, 16–28.

Wang, X., Hou, T., Wang, M., Zhang, C., Zhang, Z., Pan, R., Marxer, F. & Zhang, H. (2021). A new clinopyroxene thermobarometer for mafic to intermediate magmatic systems. *European Journal of Mineralogy* **33**, 621–637.

Wang, Z., Wilde, S. A. & Wan, J. (2010). Tectonic setting and significance of 2.3-2.1 Ga magmatic events in the Trans-North China Orogen: New constraints from the Yanmenguan mafic-ultramafic intrusion in the Hengshan-Wutai-Fuping area. *Precambrian Research*. Elsevier **178**, 27–42.

Wei, F., Pan, B. & Xu, J. (2021). Sr-Nd-Pb-Ca Isotopes of Holocene Basalts from Jingpohu, NE China: Implications for the Origin of Their Enriched Mantle Signatures. *Minerals*. MDPI AG **11**, 790.

Weng, B. Y., Hong, L. B., Zhang, Y. H., Zhang, L., Xu, Y. G., Yuan, C. & He, P. L. (2022). Petrological evidence of an anhydrous carbonatitic peridotite source for the Xiaogulihe ultrapotassic volcanic rocks, northeastern China. *Lithos*. Elsevier **426–427**, 106776.

Wilson, M. (1989). *Igneous Petrogenesis*. *Igneous Petrogenesis*. Dordrecht: Springer Netherlands.

Yoshikawa, M., Arai, S., Ishida, Y., Tamura, A. & Shimizu, Y. (2010). Trace element and Sr-Nd isotopic features of ultramafic xenoliths from Kurose, Southwest Japan. *Journal of Mineralogical and Petrological Sciences* **105**, 346–351.

Zhang, M., Suddaby, P., Thompson, R. N., Thirlwall, M. F. & Menzies, M. A. (1995). Potassic volcanic rocks in NE China: Geochemical constraints on mantle source and magma genesis. *Journal of Petrology*. Oxford Academic **36**, 1275–1303.

Zhao, D., Yanada, T., Hasegawa, A., Umino, N. & Wei, W. (2012a). Imaging the subducting slabs and mantle upwelling under the Japan Islands. *Geophysical Journal International*. Oxford University Press **190**, 816–828.

Zhao, G., Cawood, P. A., Li, S., Wilde, S. A., Sun, M., Zhang, J., He, Y. & Yin, C. (2012b). Amalgamation of the North China Craton: Key issues and discussion. *Precambrian Research*. Elsevier **222–223**, 55–76.

Zindler, A. (1986). Chemical Geodynamics. *Annual Review of Earth and Planetary Sciences* **14**, 493–571.

Zou, H., Reid, M. R., Liu, Y., Yao, Y., Xu, X. & Fan, Q. (2003). Constraints on the origin of historic potassic basalts from northeast China by U–Th disequilibrium data. *Chemical Geology*. Elsevier **200**, 189–201.